
HUMAN–AI ENSEMBLES IMPROVE DEEPFAKE DETECTION IN LOW-TO-MEDIUM QUALITY VIDEOS

Marco Postiglione, Isabel Gortner, V. S. Subrahmanian
 Northwestern University
 vss@northwestern.edu

ABSTRACT

Deepfake detection is widely framed as a machine learning problem, yet how humans and AI detectors compare under realistic conditions remains poorly understood. We evaluate 200 human participants and 95 state-of-the-art AI detectors across two datasets: DF40, a standard benchmark, and CharadesDF, a novel dataset of videos of everyday activities. CharadesDF was recorded using mobile phones leading to low/moderate quality videos compared to the more professionally captured DF40. Humans outperform AI detectors on both datasets, with the gap widening in the case of CharadesDF where AI accuracy collapses to near chance (0.537) while humans maintain robust performance (0.784). Human and AI errors are complementary: humans miss high-quality deepfakes while AI detectors flag authentic videos as fake, and hybrid human-AI ensembles reduce high-confidence errors. These findings suggest that effective real-world deepfake detection, especially in non-professionally produced videos, requires human–AI collaboration rather than AI algorithms alone.

CONTENTS

1	Introduction	2
2	Results	4
2.1	Research Question 1: Human vs. AI Detection Performance	5
2.2	Research Question 2: Ensemble Aggregation and Human–AI Complementarity . . .	5
2.3	Research Question 3: Visual Quality Factors and Detection Performance	9
2.4	Research Question 4: Confidence, Calibration, and Metacognition	12
2.5	Research Question 5: Demographic Predictors of Detection Accuracy	14
3	Discussion	16
3.1	Limitations and future directions	18
3.2	Ethical and societal impact	18
4	Methods	19
4.1	Consent and ethics	19
4.2	Digital experiment interface	20
4.3	Experiment stimuli	20
4.4	Participants	21
4.5	Randomization	21

4.6	Quality Features Extraction	21
4.7	AI detectors	26
5	Data availability	26
6	Code availability	26
7	Acknowledgments	36
8	Author contributions	36
9	Competing interests	36
A	Supplementary Information	37
A.1	RQ1: Video-level performance	37
A.2	RQ2: Additional ensemble techniques	38
A.3	RQ3: Performance curves by quality feature	39

1 INTRODUCTION

The emergence of deepfake technology (i.e., artificial intelligence systems capable of generating synthetic media depicting events that may have never occurred) has fundamentally altered the landscape of digital trust (Rössler et al., 2019; Li et al., 2020; Yan et al., 2024b; Köbis et al., 2021; Appel and Prietzel, 2022; Sanchez-Acedo et al., 2024a). From non-consensual intimate imagery to political disinformation campaigns, deepfakes have been linked to various negative effects (Cuevas and Ribeiro, 2026; Köbis et al., 2021; Preu et al., 2022; Appel and Prietzel, 2022; Sanchez-Acedo et al., 2024a). As generative AI capabilities continue to advance at a remarkable pace, the question of how society can reliably distinguish authentic from synthetic media has become increasingly urgent (Cooke et al., 2025; Frank et al., 2023; Kamali et al., 2025).

In early 2025, a US judge asked us to produce a deepfake video of him chopping wood. He sent us a real video, and we produced deepfake versions where the judge’s face was swapped with the face of two consenting individuals. AI algorithms were unable to correctly classify the fake videos. We hypothesized that this may have been due to several factors: (i) the source footage was recorded in an open space with substantial camera movement and frequent zooming in and out. (ii) There were also frames in which the subject’s face was only partially visible (e.g., when bringing axe down from above the head to the chopping block). (iii) The face itself was not always very large in size. These conditions are typical of authentic user-generated content but largely absent from existing detection benchmarks. The resulting deepfakes proved difficult for both human observers and state-of-the-art AI detectors to identify as fake, underscoring that detection performance measured on high-quality, well-framed benchmark videos may not transfer to the kinds of footage that a normal citizen might record with their mobile phone or similar device.

Despite the extensive focus on AI-based detection, relatively little systematic research has examined how *humans* perform at detecting deepfakes, or whether human and AI detection capabilities might be combined to achieve more robust detection. Existing work shows that humans often struggle to detect deepfakes or other AI-generated media, with performance frequently hovering near chance (Köbis et al., 2021; Bray et al., 2022; Cooke et al., 2025; Frank et al., 2023; Hashmi et al., 2024; Müller et al., 2021; Jin et al., 2025). Prior studies have documented that humans struggle to detect deepfakes under some conditions, but these findings are typically based on small stimulus sets, controlled laboratory conditions, or specific forgery techniques that may not generalize (Bray et al., 2022; Preu et al., 2022; Pehlivanoglu et al., 2026; Josephs et al., 2023; Jin et al., 2025). At the same time, comparisons of human and AI-based detection have yielded mixed results: some works report automated detectors clearly outperforming humans on standard benchmarks (Rössler et al.,

2019; Korshunov and Marcel, 2021; Hashmi et al., 2024), whereas others find human observers matching or even exceeding model performance in certain regimes or modalities (Groh et al., 2021; Goh et al., 2024; Pehlivanoglu et al., 2026; Müller et al., 2021). *The field lacks comprehensive, head-to-head comparisons of human and AI detection across datasets that vary systematically in their realism and difficulty.*

This paper addresses these gaps through a comprehensive empirical investigation comparing human and AI deepfake detection. We evaluate 200 human participants and 95 state-of-the-art AI deepfake detectors spanning several architectural paradigms including frequency-based methods (Qian et al., 2020; Liu et al., 2021; Luo et al., 2021), attention mechanisms (Zhao et al., 2021a; Dang et al., 2020), reconstruction-based approaches (Cao et al., 2022), contrastive learning (Yan et al., 2023a; Zhao et al., 2021b), and transformer architectures (Zhuang et al., 2022; Bertasius et al., 2021), on two complementary datasets.

The first dataset is DF40 (Yan et al., 2024b), a recently published benchmark featuring state-of-the-art deepfakes of YouTube-sourced videos. DF40 and similar benchmarks typically feature well-lit subjects in frontal poses with consistently visible faces (Rössler et al., 2019; Li et al., 2020). These conditions diverge substantially from authentic user-generated content, where variability in camera movement, lighting, occlusion, and camera angle is the norm (Josephs et al., 2023; Cooke et al., 2025; Frank et al., 2023). This gap matters because real-world detection (e.g., in legal proceedings, at protest marches and/or civic events) frequently involves videos depicting ordinary activities such as nodding in agreement, entering a building, or signing a document. Such recordings might be fabricated to incriminate, or genuine footage might be dismissed as synthetic by those seeking to evade accountability.

To address this gap, we developed CharadesDF, a novel dataset of authentic home recordings and corresponding deepfakes (Figure 1). The name derives from the Charades dataset (Sigurdsson et al., 2016), a video corpus of everyday indoor activities whose name alludes to the parlor game of acting out scenes. We sourced our activity instructions from Charades, asking participants to perform scripted actions such as drinking from a coffee cup, opening a closet, and moving around rooms in their homes. We recruited participants via an IRB-approved study and generated deepfakes using publicly available face-swapping tools, simulating the realistic scenario of non-experts creating synthetic media with accessible software (Tahir et al., 2021; Preu et al., 2022).

We address five research questions:

- RQ1 How does human detection accuracy compare to state-of-the-art AI detectors?** Prior studies have typically compared humans to a small number of AI detectors on a single dataset or modality (Groh et al., 2021; Korshunov and Marcel, 2021; Hashmi et al., 2024; Müller et al., 2021; Goh et al., 2024), leaving open how these comparisons generalize across different architectures and recording conditions.
- RQ2 Does combining multiple assessments improve detection, and do humans and AI detectors contribute complementary strength?** Earlier work suggests that ensembles of human crowds and models can outperform either alone, but are vulnerable to automation bias and misleading AI advice (Groh et al., 2021; Boyd et al., 2023; Josephs et al., 2023; Ibsen et al., 2024; Casu et al., 2025). We extend this line of inquiry by systematically aggregating predictions made by varied model families with human assessments across both controlled and realistic datasets.
- RQ3 How do video quality factors (e.g., face size, lighting, image noise, and pose variation) influence deepfake detection performance?** Existing results indicate that compression, channel noise, and viewing conditions strongly modulate both human and AI accuracy (Rössler et al., 2019; Prasad et al., 2022; Josephs et al., 2023; Wöhler et al., 2021), but their relative impact across AI detector classes and human observers under realistic, heterogeneous content remains poorly understood.
- RQ4 What is the relationship between confidence and accuracy in deepfake detection?** Prior work has documented substantial miscalibration, including truth bias, Dunning–Kruger effects, and conflict detection signals when people misclassify convincing fakes (Köbis et al., 2021; Miller et al., 2023; Janssen et al., 2024; Chen and Goh, 2025; Casu et al., 2025). We examine whether similar patterns arise in our setting and how confidence (in either the human’s prediction or an AI detector’s prediction) is related

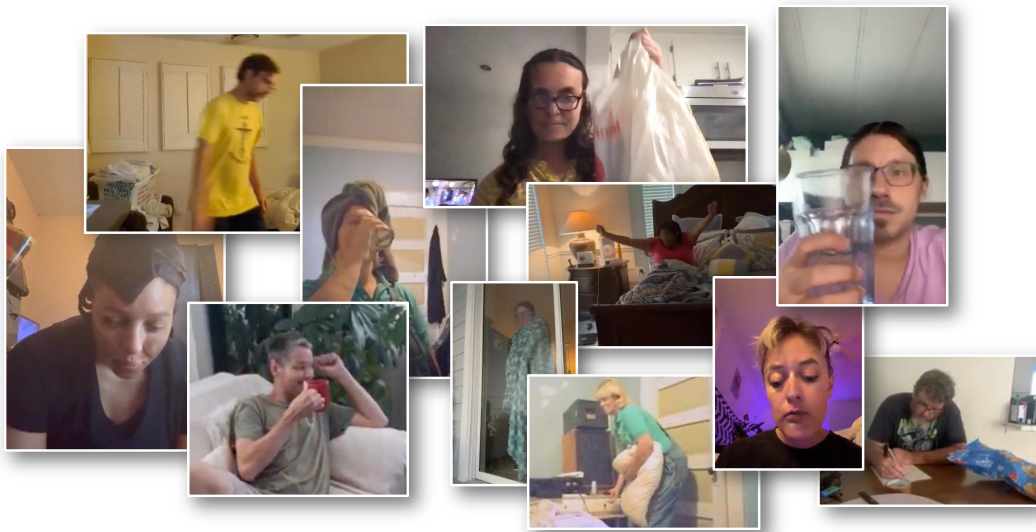


Figure 1: **Examples of video recordings from the CharadesDF dataset.** Participants recorded videos in their home environments while performing everyday activities such as drinking from cups, holding objects, stretching, and working at desks. These conditions produce substantial variability in lighting, camera angles, face visibility, and image quality—challenges common in authentic user-generated content but underrepresented in existing deepfake detection benchmarks.

to prediction accuracy in the two datasets (DF40 which has relatively quality video, and CharadesDF which has relatively low/moderate quality video).

RQ5 Do demographic characteristics predict individual differences in deepfake detection performance? Recent studies have linked detection ability to factors such as age, analytic thinking, media literacy, and face-recognition aptitude, with generally small-to-moderate effect sizes and mixed findings (Frank et al., 2023; Pehlivanoglu et al., 2026; Mink et al., 2024; Alsobeh et al., 2024; Davis et al., 2025; Müller et al., 2021; Xie, 2025). We test whether demographic variables explain variance in performance in our more ecologically realistic setting.

Our findings demonstrate that humans substantially outperform AI detectors, particularly under realistic conditions where AI detectors approach chance-level performance, extending and qualifying prior mixed evidence on human–AI comparisons (Rössler et al., 2019; Groh et al., 2021; Korshunov and Marcel, 2021; Hashmi et al., 2024; Goh et al., 2024; Pehlivanoglu et al., 2026). We found that human and AI errors are complementary, enabling hybrid ensembles involving both humans and AI detectors to eliminate highly-confident errors, consistent with prior work (Groh et al., 2021; Boyd et al., 2023; Ibsen et al., 2024). Finally, we find that most human demographic factors do not reliably predict human detection ability, suggesting that human performance depends on factors beyond general demographics and technological proficiency (Jin et al., 2025; Frank et al., 2023; Davis et al., 2025). Together, these results indicate that the optimal approach to real-world deepfake detection may not be more sophisticated machine learning, but rather an ensemble of human and AI detectors that leverages complementary strengths (Groh et al., 2021; Josephs et al., 2023; Ibsen et al., 2024), especially when the videos are of low/medium quality.

2 RESULTS

We conducted two complementary experiments to compare human and AI deepfake detection capabilities. For AI detection evaluation, we trained 32 state-of-the-art deepfake detection architectures on three training datasets (i.e., FaceForensics++ (Rössler et al., 2019), CelebDF-v2 (Li et al., 2020),

and the DF40 training split (Yan et al., 2024b)) yielding 96 detector variants (with one excluded due to architectural incompatibility). Each variant was evaluated on two test sets: a sample of 1,000 videos from the held-out DF40 test set (500 real, 500 fake across 10 forgery techniques) and CharadesDF, a novel dataset we developed comprising 1,000 videos (500 authentic home recordings and 500 corresponding deepfakes generated using five face-swapping models). The DF40 sample features YouTube-sourced videos with subjects in predominantly frontal poses and consistently visible faces, while CharadesDF was designed to simulate challenging real-world conditions. Participants recorded videos in their home environments using personal devices while following scripted activity instructions, resulting in greater variability in image quality, camera angles, and face visibility.

For human evaluation, we conducted two IRB-approved studies via the Prolific platform, recruiting 100 participants for each dataset. Due to practical constraints on participant time, each participant viewed a randomly sampled subset of 60 videos from the corresponding 1,000-video pool, ensuring each video received multiple independent ratings. Participants rated their confidence that each video was fabricated on a 5-point Likert scale, which we converted to continuous probability scores ($p \in [0, 1]$, where $p = 1$ indicates maximum confidence in fabrication). We computed accuracy as the proportion of correct binary classifications at the $p = 0.5$ threshold, along with AUC and F1 scores on the “deepfake” class. No overlap exists between training and evaluation data for any detector, and Phase 1 participants (who recorded CharadesDF videos) were excluded from Phase 2 evaluation to prevent familiarity effects. Further details on dataset construction, model training, quality feature extraction, and participant demographics are provided in the Methods section.

2.1 RESEARCH QUESTION 1: HUMAN VS. AI DETECTION PERFORMANCE

How does human detection accuracy compare to state-of-the-art AI detectors?

TL;DR (RQ1)

1. **Humans outperform AI at detecting deepfakes.** Across both datasets and analysis levels, human participants achieved significantly higher accuracy than AI detectors.
2. **AI detectors performance degrades more on challenging datasets.** On CharadesDF, AI deepfake detectors performed near chance level ($\mu = 0.537$), while humans maintained stronger accuracy ($\mu = 0.784$), suggesting AI detectors are more sensitive to dataset characteristics.

We compared performance at the participant level, treating each human participant and each AI classifier as an individual detector. Figure 2 displays the distribution of accuracy scores across all participants and classifiers for both datasets. Supplementary Figure 8 complements this analysis with aggregated predictions at the video level.

On DF40 (Figure 2A), human participants achieved a mean accuracy of 0.743 (SD = 0.122), significantly outperforming AI detectors ($\mu = 0.610$, SD = 0.143), $t(193) = 6.970$, $p < .001$, Cohen’s $d = 0.999$. This performance gap widened substantially on CharadesDF (Figure 2B), where humans maintained robust accuracy ($\mu = 0.784$, SD = 0.132) while AI detectors collapsed to near-chance performance ($\mu = 0.537$, SD = 0.043), $t(193) = 17.389$, $p < .001$, Cohen’s $d = 2.491$. AI detectors in Figure 2B are narrowly concentrated around 50%, indicating that the challenging, naturalistic conditions of CharadesDF rendered AI detection essentially ineffective. The reduced variance among AI detectors on CharadesDF (SD = 0.043 vs. 0.143 on DF40) suggests that varied architectural approaches converged to similar failure modes when confronted with realistic recording conditions.

2.2 RESEARCH QUESTION 2: ENSEMBLE AGGREGATION AND HUMAN-AI COMPLEMENTARITY

Does combining multiple assessments improve detection, and do humans and AI detectors contribute complementary strength?

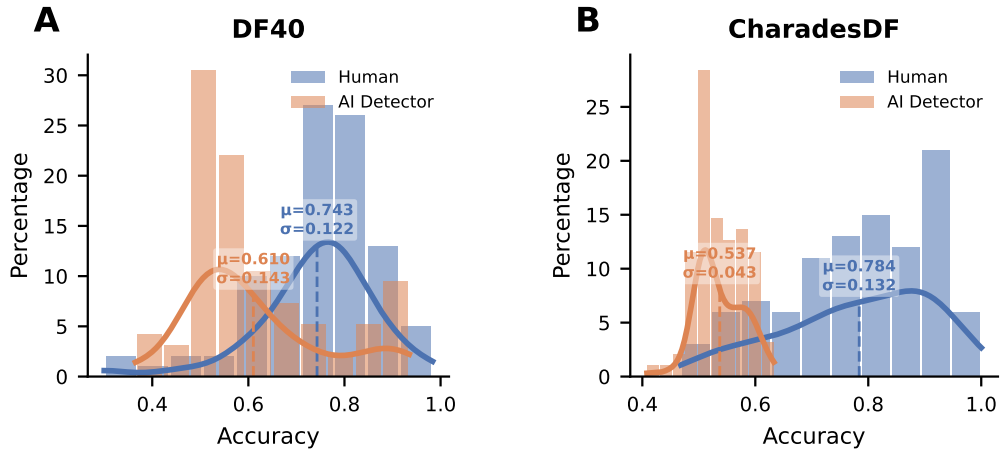


Figure 2: **Distribution of participant-level accuracy for human participants and AI detectors.** (A) DF40 dataset. (B) CharadesDF dataset. Each data point represents one participant’s overall accuracy across all videos they evaluated.

TL;DR (RQ2)

1. **Aggregating assessments substantially improves detection accuracy.** Human ensembles outperformed individual humans by 14–15 percentage points, while AI ensembles improved by 7–26 percentage points depending on dataset.
2. **Ensemble methods dramatically reduce high-confidence mistakes.** Individual judges were confidently wrong in 17–32% of cases; ensembles reduced this to under 2%, with hybrid human-AI ensembles eliminating such errors entirely.
3. **Human and AI errors do not overlap.** When humans made high-confidence errors, AI detectors tended to be correct, and vice versa.
4. **Humans and AI detectors fail in qualitatively different ways.** Humans predominantly misclassify deepfakes as real, while AI detectors predominantly misclassify real videos as deepfakes.
5. **AI ensemble gains are sensitive to domain shift.** Ensembles of AI detectors improved markedly on DF40 but showed modest gains on CharadesDF, reflecting vulnerability to distribution shift from training data.
6. **Hybrid ensembles leverage complementary failure patterns.** By combining human and AI predictions, hybrid ensembles exploit the fact that when one group fails, the other typically succeeds.

To assess whether aggregating assessments could improve detection accuracy, we compared individual performance against ensemble methods that combined predictions within and across human and AI judges (Table 1). We report accuracy, F1 score, area under the ROC curve (AUC), and catastrophic failure rate (CFR). CFR is defined as the proportion of predictions with absolute error exceeding 0.7, capturing cases where confident predictions were fundamentally wrong. This metric is conceptually related to the complement of threshold accuracy measures (Eigen et al., 2014), where the proportion of predictions falling within an acceptable error bound is reported. Here, we instead measure the proportion exceeding it, emphasizing tail failures. We experimented with CFR at multiple thresholds, spanning from 0.5 to 1.

For ensemble aggregation, we employed quality-weighted voting, which assigns greater influence to more accurate judges. To avoid circularity, we computed weights using a leave-one-out procedure. Specifically, for judge j predicting video v , the weight $w_j^{(-v)}$ reflects that judge’s accuracy on all

Table 1: **Comparison of individual versus ensemble performance on deepfake detection.** Values shown as point estimate \pm error. Error represents half-width of 95% bootstrap CI. CFR = Catastrophic Failure Rate. Bold indicates best ensemble performance.

	DF40				CharadesDF			
	Accuracy	F1	AUC	CFR	Accuracy	F1	AUC	CFR
Human (indiv.)	0.743 \pm 0.023	0.759 \pm 0.020	0.823 \pm 0.020	0.190 \pm 0.017	0.784 \pm 0.027	0.783 \pm 0.027	0.846 \pm 0.024	0.171 \pm 0.025
AI detector (indiv.)	0.610 \pm 0.030	0.612 \pm 0.042	0.686 \pm 0.037	0.279 \pm 0.036	0.537 \pm 0.009	0.533 \pm 0.041	0.583 \pm 0.014	0.317 \pm 0.029
Human ensemble	0.890 \pm 0.020	0.888 \pm 0.021	0.952 \pm 0.013	0.019 \pm 0.009	0.928 \pm 0.017	0.926 \pm 0.019	0.979 \pm 0.009	0.010 \pm 0.007
AI ensemble	0.869 \pm 0.020	0.876 \pm 0.021	0.949 \pm 0.012	0.001 \pm 0.002	0.607 \pm 0.033	0.683 \pm 0.034	0.697 \pm 0.035	0.009 \pm 0.006
Hybrid ensemble	0.941 \pm 0.014	0.941 \pm 0.014	0.988 \pm 0.005	0.000 \pm 0.000	0.924 \pm 0.018	0.924 \pm 0.019	0.979 \pm 0.008	0.000 \pm 0.000

videos *except* v :

$$w_j^{(-v)} = \frac{1}{|V_j| - 1} \sum_{v' \in V_j \setminus \{v\}} \mathbf{1}[\hat{y}_{j,v'} = y_{v'}] \quad (1)$$

where V_j is the set of videos evaluated by judge j , $\hat{y}_{j,v'}$ is the binarized prediction (threshold = 0.5), and $y_{v'}$ is the ground truth label. The ensemble prediction for video v is then the weighted average of probability scores:

$$p_v^{\text{ensemble}} = \frac{\sum_j w_j^{(-v)} \cdot p_{j,v}}{\sum_j w_j^{(-v)}} \quad (2)$$

where $p_{j,v} \in [0, 1]$ is judge j 's raw probability score for video v . For hybrid human–AI ensembles, we used a two-stage hierarchical aggregation to prevent the larger group from dominating the final prediction. First, predictions were aggregated separately within human and AI groups using quality-weighted voting (Equations 1–2), yielding group-level predictions p_v^{human} and p_v^{AI} . These group-level predictions were then combined with equal weighting:

$$p_v^{\text{hybrid}} = \frac{1}{2} (p_v^{\text{human}} + p_v^{\text{AI}}) \quad (3)$$

This balanced approach ensures that the complementary strengths of human intuition and algorithmic pattern detection contribute equally to the final prediction, regardless of the number of judges in each group. Results using alternative aggregation strategies (simple averaging, median voting, and majority voting) are provided in Supplementary Tables 11–14.

Quantifying ensemble gains across aggregation methods Individual human judges achieved moderate accuracy (DF40: 0.743, 95% CI [0.718, 0.766]; CharadesDF: 0.784, 95% CI [0.758, 0.810]), while individual AI detectors performed at or near chance levels (DF40: 0.610, 95% CI [0.583, 0.639]; CharadesDF: 0.537, 95% CI [0.529, 0.546]; Table 1). Aggregating assessments within each group yielded substantial improvements. Human ensembles reached 0.890 (95% CI [0.870, 0.909]) on DF40 and 0.928 (95% CI [0.909, 0.945]) on CharadesDF—absolute improvements of 14.7 and 14.4 percentage points over individual humans, respectively (DF40: $t(263) = 9.35$, $p < 0.001$, Cohen’s $d = 0.62$; CharadesDF: $t(214) = 8.94$, $p < 0.001$, Cohen’s $d = 0.70$). AI ensembles improved markedly on DF40 (0.869, 95% CI [0.848, 0.889]; +25.8 percentage points; $t(214) = 14.19$, $p < 0.001$, Cohen’s $d = 0.99$), though gains on CharadesDF were more modest (0.607, 95% CI [0.573, 0.641]; +7.0 percentage points; $t(851) = 3.89$, $p < 0.001$, Cohen’s $d = 0.20$), likely reflecting the domain shift from training data that disproportionately affected algorithmic detectors.

High-confidence error analysis Beyond improving average accuracy, ensemble methods dramatically reduced catastrophic failures. Individual humans exhibited catastrophic failure rates of 19.0% (DF40) and 17.0% (CharadesDF), while individual detectors failed catastrophically in 27.9% and 31.7% of cases, respectively. Human ensembles reduced these rates to 1.9% and 1.0% (Fisher’s exact test: DF40, $p < 0.001$; CharadesDF, $p < 0.001$), while AI ensembles achieved 0.1% and 0.9% (DF40, $p < 0.001$; CharadesDF, $p < 0.001$). Hybrid ensembles did not show catastrophic failures.

Characterizing human-AI error independence The effectiveness of hybrid ensembles stems from complementary failure patterns between human and AI judges (Figure 3). When we classified each video by whether human ensembles, AI ensembles, or both failed catastrophically, we found

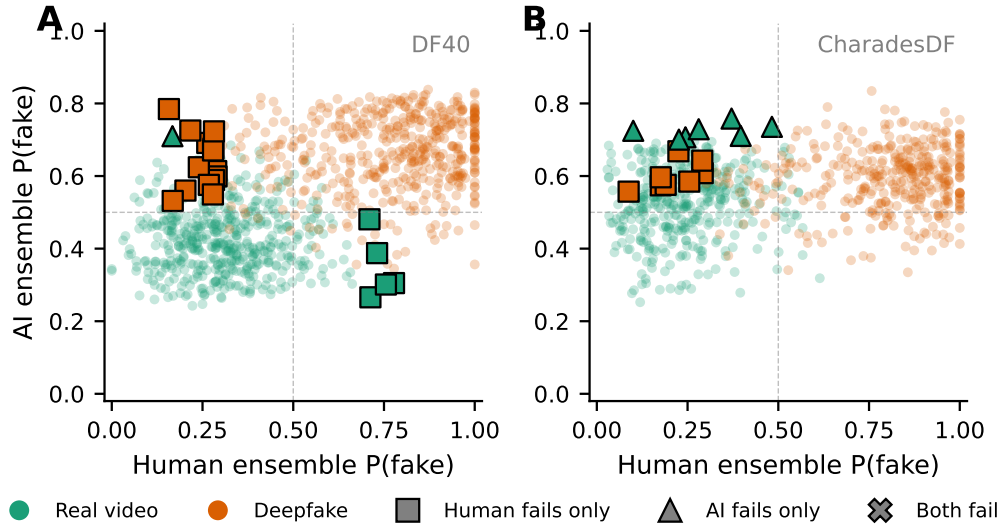


Figure 3: **Complementary failure patterns between human and AI ensembles.** Each point represents a video, plotted by human ensemble probability (x-axis) versus AI ensemble probability (y-axis) of being a deepfake. Dashed lines indicate the decision threshold (0.5). Small circles show videos without catastrophic failures (teal: real videos; orange: deepfakes). Squares indicate videos where only the human ensemble failed catastrophically; triangles indicate videos where only the AI ensemble failed. No videos caused catastrophic failures in both groups simultaneously (no X markers). (A) DF40 dataset. (B) CharadesDF dataset.

no overlap: no videos caused catastrophic failures in both groups simultaneously on either dataset. The phi coefficient measuring association between human and AI failures was near zero (DF40: $\phi = -0.004$; CharadesDF: $\phi = -0.010$), confirming that errors were statistically independent (Fisher’s exact test: DF40, $p = 1.000$; CharadesDF, $p = 1.000$).

Moreover, failure patterns differed qualitatively by ground truth. When only humans failed catastrophically, they predominantly classified deepfakes as real (DF40: 14 of 19 failures, 74%; CharadesDF: 8 of 8, 100%), suggesting vulnerability to high-quality face manipulations. In contrast, AI-only failures predominantly misclassified real videos as deepfakes (DF40: 1 of 1 failures, 100%; CharadesDF: 7 of 7, 100%), potentially due to over-reliance on compression artifacts present in both authentic and manipulated content (Fisher’s exact test comparing error types: DF40 humans $p = 0.039$, AI $p = 1.000$; CharadesDF humans $p = 0.004$, AI $p = 0.015$). This complementarity explains the hybrid ensemble’s effectiveness: when humans failed, AI detectors provided correct predictions, and vice versa. By averaging predictions, hybrid ensembles leveraged this complementarity to eliminate catastrophic failures.

Robustness of ensemble benefits across threshold definitions The preceding analyses defined catastrophic failures using a threshold of 0.7 (probability errors ≥ 0.7). To assess robustness, we examined how catastrophic failure rates varied across threshold definitions from 0.5 to 1.0 (Figure 4). Across both datasets, ensemble methods consistently outperformed individual methods at every threshold examined. AI detectors exhibited the highest CFR across all thresholds, particularly on CharadesDF where CFR exceeded 47% at the most lenient threshold (0.5). Human ensembles reduced CFR substantially compared to individual humans, reaching zero failures by threshold 0.85 on DF40 and 0.95 on CharadesDF. AI ensembles reached zero failures by threshold 0.75 on DF40, though CharadesDF required threshold 0.8, reflecting the domain shift challenges that disproportionately affected algorithmic detectors. Hybrid ensembles achieved zero catastrophic failures by threshold 0.7 on both datasets, demonstrating that complementarity benefits extend beyond any particular operational definition of catastrophic failure. The AI ensemble on CharadesDF showed notably ele-

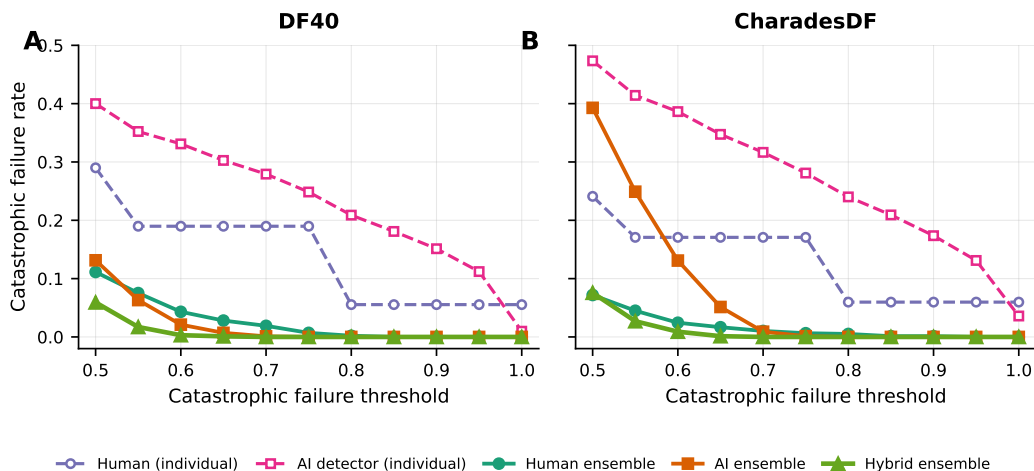


Figure 4: **Catastrophic failure rates across threshold definitions.** CFR was computed for threshold values ranging from 0.5 (any probability error ≥ 0.5 is catastrophic) to 1.0 (only complete misclassification with probability error = 1.0). Dashed lines show mean individual performance; solid lines show ensemble performance. Quality-weighted voting was used for all ensembles. (A) DF40 dataset. (B) CharadesDF dataset.

vated CFR at lenient thresholds (39.3% at 0.5), but hybrid ensembles mitigated this vulnerability by incorporating human assessments that were less susceptible to distribution shift.

2.3 RESEARCH QUESTION 3: VISUAL QUALITY FACTORS AND DETECTION PERFORMANCE

How do video quality factors influence deepfake detection performance?

TL;DR (RQ3)

- Face size is the strongest and most consistent predictor of detection accuracy.** Larger, more visible faces substantially improve performance for both humans and AI detectors.
- AI detectors are more sensitive to low-level visual quality than humans.** Factors such as signal-to-noise ratio, color balance, contrast, and overall quality primarily affect AI performance, with limited impact on humans.
- Face scaling affects AI detectors and humans differently.** Inter-ocular distance negatively impacts AI accuracy but does not significantly affect humans, indicating a specific vulnerability of AI detectors to scaling-related artifacts.
- Humans benefit from interpretable cues, such as face recognition confidence.** Higher face recognizability improves human accuracy, while AI detectors rely less on this signal.
- Some visual conditions impair humans but can help AI detectors.** For example, exaggerated facial expressions reduce human accuracy but improve AI ensemble performance, suggesting different information-processing strategies.
- Lighting and brightness effects are dataset-dependent.** For instance, increased brightness reduces AI accuracy in CharadesDF but shows no effect in DF40.
- Most other visual features have limited impact.** Variables such as blur, occlusion, facial aspect ratios, and most pose variations do not significantly influence detection after correction for multiple comparisons.

8. **Visual quality explains only a modest portion of performance.** Detection accuracy is influenced by multiple factors beyond simple visual quality, as reflected by relatively low R^2 values.

Regression analysis of visual quality predictors. To identify which visual quality characteristics influence detection performance, we conducted ordinary least squares regressions with standardized coefficients and Benjamini–Hochberg false discovery rate (FDR) correction applied per regression to account for multiple comparisons across the 20 quality features (Table 2). Standard errors were determined by Breusch–Pagan heteroscedasticity tests, with HC3 robust standard errors used where heteroscedasticity was detected ($p < 0.05$) and standard errors otherwise.

Table 2: Quality factors predicting detection accuracy.

Quality Factor	DF40					CharadesDF				
	Human	AI	Human Ens.	AI Ens.	Hybrid Ens.	Human	AI	Human Ens.	AI Ens.	Hybrid Ens.
FR Confidence	0.008*	0.001	0.001	0.011	0.002	0.024*	-0.003	0.014	-0.012	0.035*
Bbox Area (ratio)	0.046***	0.034***	0.028	0.039***	0.017	0.016	0.026**	0.000	0.038	0.003
Face Presence (ratio)	-0.008	0.002	-0.006	-0.011*	-0.002	0.008	0.002	0.010	-0.001	0.008
IOD	-0.029	-0.057***	0.019	-0.029	0.003	-0.022	-0.062***	0.026	-0.106**	-0.004
Left EAR	-0.001	-0.002	-0.007	0.013	0.002	0.013	0.004	0.013	0.026	0.019
Right EAR	-0.004	-0.002	0.012	-0.015	-0.003	0.003	-0.005	0.016	-0.012	0.011
MAR	-0.012	0.000	-0.013	0.016	0.009	0.002	-0.010	-0.001	-0.017	-0.004
SNR	0.033*	0.040***	-0.006	0.004	0.011	0.004	0.040***	-0.013	0.084**	0.002
Brightness	0.000	-0.012	0.003	-0.004	0.000	-0.002	-0.026**	0.000	-0.043	0.000
Sharpness	-0.021	-0.001	-0.009	0.016	0.012	-0.021	-0.003	-0.008	-0.001	-0.001
Contrast	0.015	0.018**	-0.004	0.035	0.008	0.006	0.015	-0.019	0.029	-0.028
Color Balance	0.012	0.020***	-0.010	0.014	-0.002	0.007	0.018*	0.003	0.058*	-0.007
Blur (blurry)	-0.002	-0.010	-0.017	-0.015	-0.007	-0.010	-0.007	-0.013	-0.033	-0.020
Blur (hazy)	-0.006	-0.001	0.008	-0.017	0.006	0.006	-0.005	-0.011	-0.013	-0.021
Pose (profile)	0.011	-0.005	0.002	-0.010	0.001	-0.006	-0.003	-0.015	0.002	-0.012
Pose (slight angle)	0.002	0.002	0.012	-0.020	0.012	-0.006	-0.001	-0.017	0.003	-0.028*
Occlusion	-0.004	0.005	-0.022	0.001	0.005	0.002	0.001	-0.002	0.007	0.008
Exaggerated expression	0.000	0.000	0.000	0.000	0.000	-0.020*	0.005	-0.035**	0.027***	-0.032*
Extreme lighting	-0.018	-0.001	-0.015	-0.003	0.005	0.000	0.002	-0.010	0.013	-0.012
Quality Score	0.015	0.019**	0.015	-0.001	0.009	-0.011	0.016	-0.014	0.050	-0.001
R^2	0.099	0.137	0.037	0.048	0.019	0.059	0.093	0.041	0.051	0.061
N	997	997	997	997	997	779	779	779	779	779

Notes: Standardized OLS coefficients. Standard errors determined by Breusch–Pagan heteroscedasticity test: HC3 robust SEs used where heteroscedasticity detected ($p < 0.05$), standard SEs otherwise. p -values corrected for multiple comparisons using Benjamini–Hochberg FDR (per regression). * $p_{\text{FDR}} < 0.05$, ** $p_{\text{FDR}} < 0.01$, *** $p_{\text{FDR}} < 0.001$.

Face size emerged as the most robust predictor: bounding box area ratio was significantly associated with higher accuracy for humans ($\beta = 0.046$, $P_{\text{FDR}} < 0.001$), AI detectors ($\beta = 0.034$, $P_{\text{FDR}} < 0.001$), and the AI ensemble ($\beta = 0.039$, $P_{\text{FDR}} < 0.001$) in DF40, with a consistent positive effect for AI detectors in CharadesDF ($\beta = 0.026$, $P_{\text{FDR}} = 0.009$). The human ensemble effect in DF40 did not survive FDR correction ($\beta = 0.028$, $P_{\text{FDR}} = 0.245$). Inter-ocular distance (IOD) showed a strong negative association with AI accuracy that survived FDR correction in both datasets (DF40: $\beta = -0.057$, $P_{\text{FDR}} < 0.001$; CharadesDF: $\beta = -0.062$, $P_{\text{FDR}} < 0.001$), with an especially large effect in the CharadesDF AI ensemble ($\beta = -0.106$, $P_{\text{FDR}} = 0.002$), while showing no significant effects for humans after correction—suggesting that AI detectors are specifically susceptible to artifacts associated with face scaling. Signal-to-noise ratio positively predicted AI detection performance across both datasets after FDR correction (DF40: $\beta = 0.040$, $P_{\text{FDR}} < 0.001$; CharadesDF: $\beta = 0.040$, $P_{\text{FDR}} < 0.001$), with a particularly strong effect in the CharadesDF AI ensemble ($\beta = 0.084$, $P_{\text{FDR}} = 0.008$); notably, an effect for humans in DF40 also reached significance ($\beta = 0.033$, $P_{\text{FDR}} = 0.044$). Color balance showed significant positive associations with AI detection accuracy in both datasets after correction (DF40: $\beta = 0.020$, $P_{\text{FDR}} < 0.001$; CharadesDF: $\beta = 0.018$, $P_{\text{FDR}} = 0.020$) and in the CharadesDF AI ensemble ($\beta = 0.058$, $P_{\text{FDR}} = 0.017$) but not human accuracy, indicating that AI detectors leverage low-level color statistics that humans do not consciously process. Contrast significantly predicted AI detection accuracy in DF40 ($\beta = 0.018$, $P_{\text{FDR}} = 0.002$) but not in CharadesDF. The overall Quality Score—an aggregate measure of visual quality—significantly predicted AI detection accuracy in DF40 ($\beta = 0.019$, $P_{\text{FDR}} = 0.001$), but showed no significant effect in CharadesDF ($P_{\text{FDR}} = 0.145$), consistent with the pattern that AI detectors are more sensitive to overall visual quality than humans. Face recognition confidence positively predicted human accuracy in both datasets (DF40: $\beta = 0.008$, $P_{\text{FDR}} = 0.030$; CharadesDF: $\beta = 0.024$, $P_{\text{FDR}} = 0.039$) and hybrid ensemble accuracy in CharadesDF ($\beta = 0.035$,

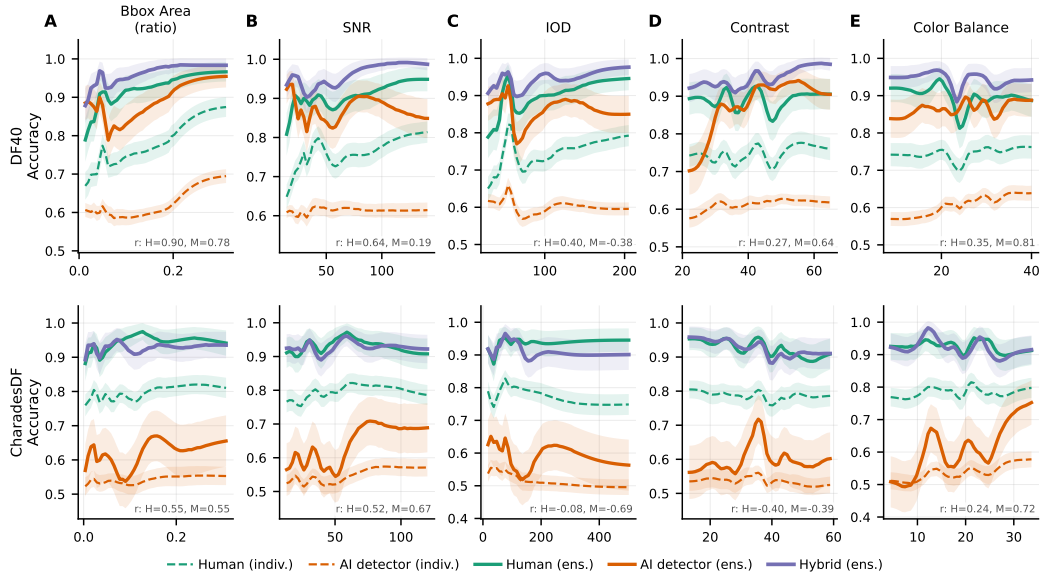


Figure 5: **Detection accuracy as a function of image quality factors.** Smoothed performance curves showing the relationship between quality features and detection accuracy for human individuals (teal, dashed), AI detectors (orange, dashed), human ensembles (teal, solid), AI ensembles (orange, solid), and hybrid ensembles (purple, solid). Shaded regions indicate 95% confidence intervals. We indicate correlations (ρ) in each subplot for both humans (H) and AI detectors (M). Rows correspond to DF40 (top) and CharadesDF (bottom) datasets. (A) Bounding box area ratio. (B) Inter-ocular distance (IOD). (C) Signal-to-noise ratio (SNR). (D) Contrast. (E) Color balance.

$P_{\text{FDR}} = 0.013$). In the DF40 AI ensemble, face presence ratio was negatively associated with accuracy ($\beta = -0.011$, $P_{\text{FDR}} = 0.042$). Notably, brightness negatively predicted AI detection accuracy in CharadesDF ($\beta = -0.026$, $P_{\text{FDR}} = 0.009$), an effect not observed in DF40.

Exaggerated expression—defined by CLIB-FIQA (Ou et al., 2024) as the probability that a face displays an atypical or non-neutral expression—emerged as a notable predictor specifically in the CharadesDF dataset, with divergent effects across detector types: it negatively predicted human accuracy ($\beta = -0.020$, $P_{\text{FDR}} = 0.046$), human ensemble accuracy ($\beta = -0.035$, $P_{\text{FDR}} = 0.004$), and hybrid ensemble accuracy ($\beta = -0.032$, $P_{\text{FDR}} = 0.013$), while positively predicting AI ensemble accuracy ($\beta = 0.027$, $P_{\text{FDR}} < 0.001$). This pattern suggests that exaggerated expressions may introduce visual complexity that impairs human judgment while providing exploitable patterns for AI detectors. Additionally, pose (slight angle) negatively predicted hybrid ensemble accuracy in CharadesDF ($\beta = -0.028$, $P_{\text{FDR}} = 0.029$).

Several other factors showed raw significance that did not survive FDR correction, including sharpness for humans (DF40: $P_{\text{FDR}} = 0.077$; CharadesDF: $P_{\text{FDR}} = 0.133$), extreme lighting for humans in DF40 ($P_{\text{FDR}} = 0.098$), and contrast for AI detectors in CharadesDF ($P_{\text{FDR}} = 0.221$). The remaining quality features—including left and right eye aspect ratios, mouth aspect ratio, blur variables, most pose variables, and occlusion—did not reach significance after FDR correction in any model. The overall models explained modest variance ($R^2 = 0.02$ – 0.14), consistent with quality factors representing one of multiple determinants of detection success.

Performance curves by quality feature. To complement the regression analysis, we examined how detection accuracy varies across the range of each quality factor using smoothed performance curves (Figure 5). Curves for all the remaining quality features are reported in Supplementary Material.

Face size (bounding box area ratio) showed the strongest positive relationship with accuracy for both humans ($\rho = 0.90$) and AI detectors ($\rho = 0.78$) in DF40, with human accuracy increas-

ing from approximately 67% at small face sizes to 87% at large face sizes, compared to a similar but weaker trend for AI detectors (61% to 69%). This pattern was attenuated but still present in CharadesDF ($\rho_{\text{human}} = 0.55$, $\rho_{\text{AI}} = 0.55$), with both showing parallel improvements across the feature range. Inter-ocular distance (IOD) exhibited a notably divergent pattern in DF40: human accuracy increased with IOD ($\rho = +0.40$) while AI detection accuracy decreased ($\rho = -0.38$), consistent with the regression finding that AI detectors are specifically susceptible to face-scaling artifacts. This divergence was even more pronounced in CharadesDF, where AI detectors showed a strong negative correlation with IOD ($\rho_{\text{AI}} = -0.69$) while humans showed near-zero correlation ($\rho_{\text{human}} = -0.08$), with AI detection accuracy declining from approximately 54% at low IOD to 50% at high IOD. Signal-to-noise ratio showed a strong positive correlation with human accuracy in DF40 ($\rho = 0.64$) but a much weaker relationship for AI detectors ($\rho = 0.19$); in CharadesDF, both showed positive relationships, though AI detectors exhibited a stronger correlation ($\rho = 0.67$) than humans ($\rho = 0.52$). Color balance was substantially more strongly associated with AI detection accuracy ($\rho = 0.81$ in DF40, $\rho = 0.72$ in CharadesDF) than human accuracy ($\rho = 0.35$ and $\rho = 0.24$, respectively), reinforcing the regression finding that AI detectors leverage low-level color statistics that humans do not consciously process. Contrast showed mixed patterns: in DF40, AI detectors exhibited a stronger positive relationship ($\rho = 0.64$) compared to humans ($\rho = 0.27$), while in CharadesDF both showed moderate negative correlations ($\rho_{\text{human}} = -0.40$, $\rho_{\text{AI}} = -0.39$). Across all features and datasets, the hybrid ensemble consistently achieved the highest accuracy, demonstrating that complementary insights from humans and AI detectors can be leveraged regardless of quality conditions.

2.4 RESEARCH QUESTION 4: CONFIDENCE, CALIBRATION, AND METACOGNITION

What is the relationship between confidence and accuracy in deepfake detection?

TL:DR (RQ4)

1. **Humans have better insight into when they are wrong.** Human confidence is substantially higher on correct predictions than incorrect ones, indicating genuine metacognitive awareness. AI detectors show much weaker confidence discrimination, meaning their confidence scores are less informative about prediction-level accuracy.
2. **Both humans and AI detectors show the same asymmetric calibration pattern.** Both groups are overconfident when predicting a video is real but underconfident when predicting a deepfake, despite comparable overall calibration error.
3. **The Dunning-Kruger effect appears in both humans and AI detectors.** Poor performers overestimate their ability while top performers tend toward underconfidence. This pattern is consistent across datasets and is more pronounced in AI detectors than humans.
4. **Self-reported confidence before the task does not predict actual performance.** Participants' pre-task beliefs about their deepfake detection ability bear no relationship to their actual accuracy.

Confidence discrimination and calibration analysis. Participants and models rated each video on a 5-point scale from “Definitely Authentic” to “Definitely a Deepfake,” which we converted to a probability score $p \in [0, 1]$ where 1 indicates maximum confidence that the video is a deepfake. We operationalized *confidence* as certainty in the binary prediction: $\text{confidence} = \max(p, 1 - p)$, yielding values in $[0.5, 1.0]$. For example, ratings of $p = 0.9$ (likely deepfake) or $p = 0.1$ (likely real) both yield confidence = 0.9, reflecting high certainty regardless of direction; $p = 0.5$ corresponds to minimal confidence.

Human participants demonstrated strong *confidence discrimination*: mean confidence was significantly higher on correct predictions than incorrect predictions (DF40: $\mu = 0.874$ vs. $\mu = 0.738$, $t = 29.89$, $p < 0.001$, Cohen’s $d = 0.88$; CharadesDF: $\mu = 0.901$ vs. $\mu = 0.767$, $t = 26.64$, $p < 0.001$, $d = 0.92$), indicating genuine insight into performance on individual predictions. By contrast, AI detectors showed markedly weaker confidence discrimination (DF40: $\mu = 0.845$ vs.

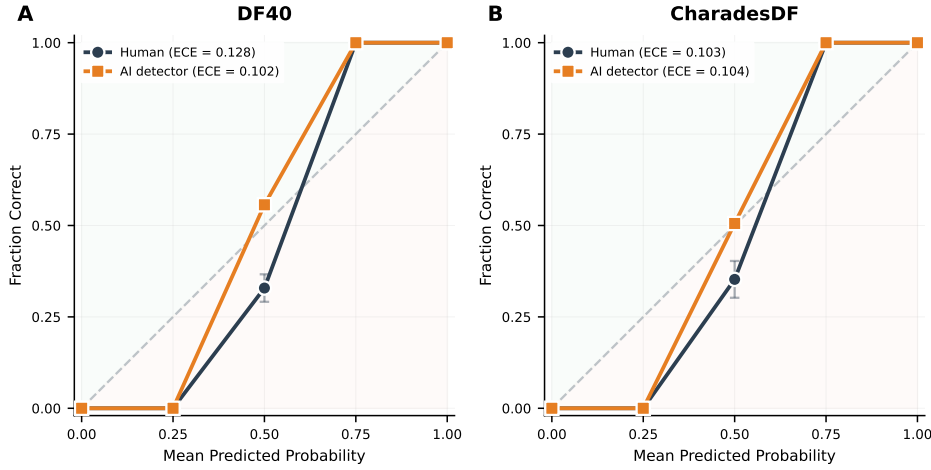


Figure 6: **Reliability diagrams for deepfake detection confidence: humans vs. AI detectors.** Calibration curves showing the relationship between mean predicted probability and fraction correct for human participants (dark curves) and AI detectors (orange curves). The dashed line indicates perfect calibration; points above the line indicate underconfidence, points below indicate overconfidence. Error bars show 95% confidence intervals. (A) DF40, (B) CharadesDF.

$\mu = 0.806$, $t = 36.15$, $p < 0.001$, $d = 0.24$; CharadesDF: $\mu = 0.815$ vs. $\mu = 0.798$, $t = 13.69$, $p < 0.001$, $d = 0.10$), suggesting that AI detectors’ confidence scores carry less diagnostic information about prediction-level correctness.

We next examined *calibration*, i.e. whether confidence magnitude corresponds to actual accuracy. Calibration determines whether confidence can serve as a reliable signal for downstream decisions, such as a content moderator prioritizing low-confidence flags or a hybrid system weighting assessments by stated certainty. A well-calibrated observer reporting 80% confidence should be correct 80% of the time. We constructed reliability diagrams by binning trials by predicted probability and computing accuracy within each bin (Figure 6), quantifying miscalibration using Expected Calibration Error ($ECE = \sum_b \frac{n_b}{N} |\text{accuracy}_b - \text{confidence}_b|$, where n_b is trials in bin b , (Naeni et al., 2015)) and Brier score (mean squared error between predictions and outcomes, (Glenn et al., 1950)).

Humans and AI detectors showed comparable overall miscalibration (DF40: human ECE = 0.128, Brier = 0.053; AI detectors ECE = 0.102, Brier = 0.056; CharadesDF: human ECE = 0.103, Brier = 0.041; AI detectors ECE = 0.104, Brier = 0.065), with a shared asymmetric pattern: both groups were overconfident when predicting a video was real (accuracy below the diagonal) but underconfident when predicting a deepfake (accuracy above the diagonal).

Overconfidence by performance quartile. We tested whether poor performers overestimate their ability relative to top performers. We computed an *overconfidence score* for each participant or model: $\text{overconfidence} = \frac{\text{confidence} - 0.5}{0.5} - \text{accuracy}$, where the normalization maps confidence from $[0.5, 1.0]$ to $[0, 1]$ for direct comparison with accuracy. Positive values indicate overconfidence; negative values indicate underconfidence. Participants and models were grouped into quartiles by accuracy (Figure 7).

Among humans in DF40, the bottom quartile (accuracy: 0.30–0.68, $n = 25$) showed slight overconfidence (+0.007), while the top quartile (accuracy: 0.81–0.98, $n = 25$) was underconfident (−0.107). The negative correlation between accuracy and overconfidence was highly significant (Spearman $\rho = -0.405$, $p < 0.001$), with the bottom quartile significantly more overconfident than the top (Mann-Whitney $U = 498.5$, $p < 0.001$). This pattern replicated in CharadesDF: bottom quartile overconfidence was +0.042 versus −0.072 for the top quartile ($\rho = -0.210$, $p = 0.036$; $U = 399$, $p = 0.023$). The same Dunning-Kruger pattern emerged among AI detectors. In DF40, the worst-performing models showed pronounced overconfidence (+0.163) while top models were underconfident (−0.096; $\rho = -0.431$, $p < 0.001$; $U = 501$, $p < 0.001$). In CharadesDF, the

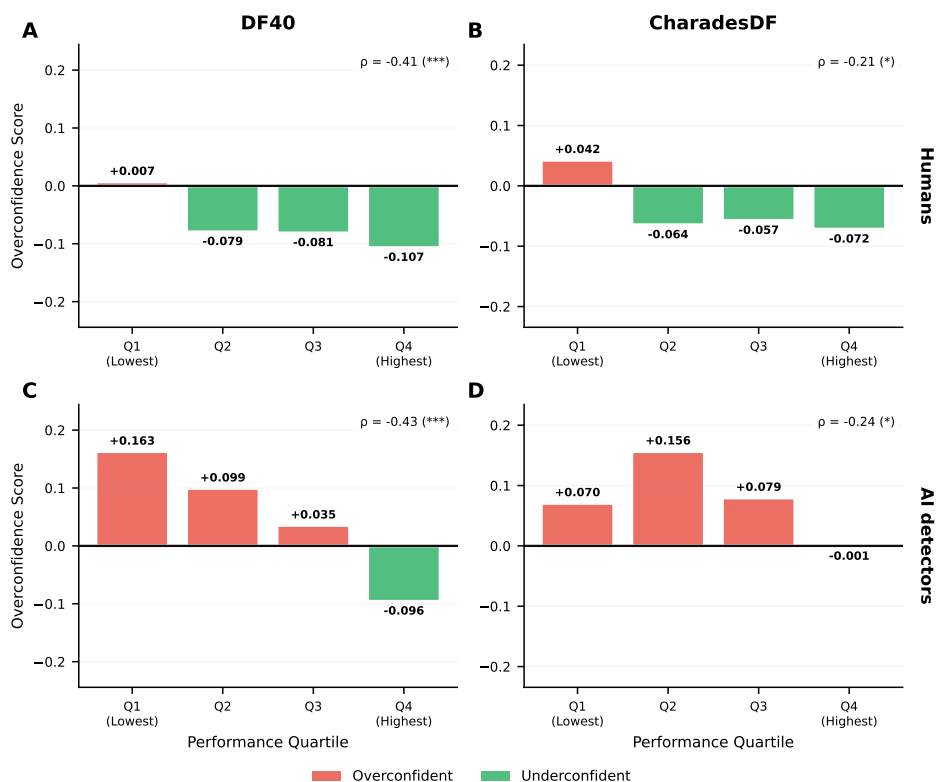


Figure 7: **Overconfidence score by performance quartile: humans vs. AI detectors.** Overconfidence computed as normalized confidence minus accuracy; positive values (red) indicate overconfidence, negative values (green) indicate underconfidence. Top row: human participants; bottom row: AI detectors. Poor performers (Q1) are overconfident while top performers (Q4) trend toward underconfidence in both groups, consistent with the Dunning-Kruger effect. The effect is more pronounced for AI detectors. (A) DF40 humans: $\rho = -0.405$, $p < 0.001$. (B) CharadesDF humans: $\rho = -0.210$, $p = 0.036$. (C) DF40 AI detectors: $\rho = -0.431$, $p < 0.001$. (D) CharadesDF AI detectors: $\rho = -0.238$, $p = 0.020$.

bottom-quartile AI detectors exhibited overconfidence (+0.070) compared to near-zero overconfidence in the top quartile (-0.001; $\rho = -0.238$, $p = 0.020$; $U = 317$, $p = 0.124$). Notably, the magnitude of the Dunning-Kruger effect was larger for AI detectors than humans in DF40: the Q1–Q4 overconfidence gap was +0.259 for AI detectors versus +0.113 for humans. In CharadesDF, this pattern reversed, with a gap of +0.071 for AI detectors versus +0.114 for humans. Self-reported confidence measured before the task (Q9: “How confident are you in your ability to detect deepfakes?”) did not predict actual accuracy for human participants (DF40: $\rho = -0.015$, $p = 0.880$; CharadesDF: $\rho = 0.062$, $p = 0.538$).

2.5 RESEARCH QUESTION 5: DEMOGRAPHIC PREDICTORS OF DETECTION ACCURACY

Do demographic characteristics predict individual differences in deepfake detection performance?

TL;DR (RQ5)

- Demographic factors explain little variance in detection accuracy.** Most demographic variables—including age, gender, tech savviness, social media usage, and deepfake familiarity—do not significantly predict performance.

Table 3: Demographic factors predicting human deepfake detection accuracy.

Demographic Factor	DF40	CharadesDF
Age	0.021	-0.025
Education	0.032	-0.043**
Tech Savviness	-0.023	0.001
Social Media Usage	0.012	0.002
Deepfake Familiarity	-0.004	0.013
Prior Deepfake Exposure	0.009	0.020
Self-Reported Confidence	0.002	-0.016
Female (vs. Male)	-0.021	0.011
R^2	0.112	0.216
N	100	100

Notes: Standardized OLS coefficients. Ordinal demographics encoded as continuous; gender dummy-encoded (reference: Male). p -values corrected using Benjamini–Hochberg FDR. * $p_{\text{FDR}} < 0.05$, ** $p_{\text{FDR}} < 0.01$, *** $p_{\text{FDR}} < 0.001$.

2. **Education shows a counterintuitive negative effect in one dataset.** Higher education was associated with lower accuracy in CharadesDF, though this effect did not replicate in DF40.
3. **Self-reported deepfake experience does not translate to better detection.** Neither familiarity with deepfakes nor prior exposure to deepfake content predicted improved accuracy.
4. **Self-assessed confidence does not predict actual performance.** Participants’ beliefs about their detection ability bore no relationship to their accuracy, consistent with the Dunning-Kruger findings in RQ4.
5. **Gender differences are absent.** Male and female participants performed comparably, with no significant differences in either dataset.

Regression analysis of demographic predictors. To examine whether individual differences in demographic characteristics predict deepfake detection performance, we conducted ordinary least squares regressions with participant-level accuracy as the dependent variable. Ordinal demographics (age, education, tech savviness, social media usage, deepfake familiarity, prior deepfake exposure, and self-reported confidence) were treated as continuous predictors; gender was dummy-encoded with male as the reference category. Coefficients were standardized, and Benjamini–Hochberg FDR correction was applied to account for multiple comparisons across the eight demographic predictors (Table 3). Standard errors were determined by Breusch–Pagan heteroscedasticity tests, with standard errors used in both datasets as no significant heteroscedasticity was detected (DF40: $p = 0.401$; CharadesDF: $p = 0.347$).

The overall models explained modest variance, with low adjusted R^2 values indicating that demographic factors account for little of the individual variation in detection performance (DF40: Adj. $R^2 = 0.024$; CharadesDF: Adj. $R^2 = 0.147$). Only one predictor survived FDR correction: education was negatively associated with accuracy in CharadesDF ($\beta = -0.043$, $P_{\text{FDR}} < 0.01$), a counterintuitive finding suggesting that more educated participants performed slightly worse. This effect did not replicate in DF40 ($\beta = 0.032$, $P_{\text{FDR}} > 0.05$), and the inconsistency across datasets suggests this may be a chance finding or reflect dataset-specific characteristics rather than a robust relationship.

Age showed no significant association with accuracy in either dataset (DF40: $\beta = 0.021$; CharadesDF: $\beta = -0.025$; both $P_{\text{FDR}} > 0.05$), contrary to common assumptions that younger, more digitally native individuals might be better at detecting synthetic media. Similarly, tech savviness (DF40: $\beta = -0.023$; CharadesDF: $\beta = 0.001$) and social media usage frequency (DF40: $\beta = 0.012$; CharadesDF: $\beta = 0.002$) were not significant predictors, indicating that general technological proficiency and exposure to social media platforms do not confer detection advantages.

Notably, neither deepfake familiarity ($\beta = -0.004$ and 0.013) nor prior deepfake exposure ($\beta = 0.009$ and 0.020) predicted accuracy in either dataset. This finding suggests that self-reported knowledge about deepfakes and experience viewing them does not translate into superior detection ability—potentially because awareness of the phenomenon does not provide the specific perceptual skills needed for accurate discrimination. Self-reported confidence in detection ability was also not significant ($\beta = 0.002$ and -0.016), consistent with our RQ4 finding that pre-task confidence does not predict actual performance.

Gender differences were absent: male and female participants performed comparably in both datasets (DF40: $\beta = -0.021$; CharadesDF: $\beta = 0.011$; both $P_{\text{FDR}} > 0.05$). The overall pattern of null findings across demographic variables suggests that deepfake detection ability may depend more on factors not captured by standard demographics—such as individual perceptual sensitivity, attention to detail, or specific training—rather than on age, education, gender, or self-reported digital media experience.

3 DISCUSSION

This paper provides comprehensive evidence from two complementary datasets and large-scale experiments with 200 human participants (100 assigned to DF40 and 100 to CharadesDF) and 95 AI detectors that humans currently outperform state-of-the-art deepfake detection algorithms, particularly under challenging real-world conditions. Our findings challenge the prevailing narrative in the deepfake detection literature that positions machine learning as the primary solution to synthetic media threats (Rössler et al., 2019; Korshunov and Marcel, 2021; Yan et al., 2023b) while revealing important opportunities for human-AI collaboration (Groh et al., 2021; Ibsen et al., 2024; Boyd et al., 2023; Josephs et al., 2023).

Humans as capable deepfake detectors. Across both controlled (DF40) and naturalistic (CharadesDF) datasets, human participants achieved significantly higher detection accuracy than AI detectors. This advantage was especially pronounced on CharadesDF, where AI detectors performed near chance level ($\mu = 0.537$) while humans maintained robust accuracy ($\mu = 0.784$). The divergence between datasets reflects the vulnerability to distribution shift of current machine learning approaches, consistent with prior work showing that detectors trained on curated benchmarks often fail under new generators, compression pipelines, or recording conditions (Rössler et al., 2019; Korshunov and Marcel, 2021; Prasad et al., 2022; Xu et al., 2025; Hasan et al., 2026; Kamali et al., 2025). AI detectors, trained on carefully curated datasets with frontal poses and consistent lighting, struggled when confronted with the variability characteristic of authentic user-generated content (e.g., the variable camera angles, partial occlusions, varied lighting conditions in CharadesDF) (Josephs et al., 2023; Cooke et al., 2025; Frank et al., 2023). Humans, by contrast, appeared to leverage more generalizable perceptual and cognitive strategies that transferred across contexts, in line with studies showing human advantages on some dynamic or ecologically rich deepfake tasks (Groh et al., 2021; Goh et al., 2024; Pehlivanoglu et al., 2026; Müller et al., 2021), even though other work has emphasized that humans detection ability can be near chance in more constrained or highly realistic regimes (Köbis et al., 2021; Bray et al., 2022; Cooke et al., 2025; Frank et al., 2023; Jin et al., 2025).

The power of ensemble methods. Our results demonstrate that aggregating multiple assessments substantially improves detection performance, with human ensembles achieving accuracy gains of 14–15 percentage points over individual humans. More striking was the dramatic reduction in high confidence errors (i.e., cases where the absolute difference between ground truth and prediction exceeds 0.7): while individual judges were confidently wrong in 17–32% of cases, ensembles reduced this to under 2%, with hybrid ensembles eliminating such errors entirely. This finding has immediate practical implications for content moderation systems, where confident misclassifications carry significant costs. It also echoes prior work showing that aggregating multiple human assessments can rival or exceed individual performance in deepfake detection (Groh et al., 2021; Jin et al., 2025) and that ensembles of human and algorithmic decisions can outperform either alone in related manipulation-detection tasks (Ibsen et al., 2024; Boyd et al., 2023; Josephs et al., 2023).

When we examined high-confidence errors, humans and AI detectors almost never failed on the same videos. Humans predominantly misclassified high-quality deepfakes as real, suggesting vul-

nerability to sophisticated face manipulations that successfully mimicked natural appearance (Köbis et al., 2021; Pehlivanoglu et al., 2026). AI detectors exhibited the opposite pattern, predominantly misclassifying real videos as deepfakes, potentially due to over-reliance on compression artifacts or low-level regularities present in both authentic and manipulated content (Rössler et al., 2019; Prasad et al., 2022; Xu et al., 2025). By combining predictions from both groups, hybrid ensembles leveraged this complementarity. This finding aligns with broader research on human–AI complementarity and collective intelligence in synthetic media detection (Groh et al., 2021; Müller et al., 2021; Boyd et al., 2023; Ibsen et al., 2024; Casu et al., 2025), while extending these principles to the specific domain of synthetic media detection at scale.

Quality factors and detection strategies. Our analysis of quality factors revealed that humans and AI detectors employ qualitatively different detection strategies. Face size emerged as the most robust predictor for both groups. Larger, more visible faces substantially improved accuracy, consistent with prior findings that visibility and pose strongly modulate human and AI performance on facial manipulations (Rössler et al., 2019; Wöhler et al., 2021; Bray et al., 2022; Nichols et al., 2022). But beyond this shared reliance on basic visibility, the groups diverged. AI detectors were significantly more sensitive to low-level visual properties: signal-to-noise ratio, color balance, and contrast all predicted AI but not human accuracy. This pattern suggests AI detectors have learned to exploit statistical regularities in image quality and compression that may not generalize across contexts (Prasad et al., 2022; Xu et al., 2025; Kamali et al., 2025), while humans rely on higher-level perceptual and semantic cues such as motion coherence, expression dynamics, and content plausibility (Wöhler et al., 2021; Gupta et al., 2020; Goh, 2024b).

These findings have implications for both attack and defense strategies. Adversaries seeking to evade AI detection might focus on matching the low-level statistical properties of authentic content, as suggested by work on benchmark shortcut learning and mirage models (Xu et al., 2025; Hasan et al., 2026; Kamali et al., 2025), while those targeting human judges might invest in high-quality face manipulations that preserve natural appearance and plausible motion (Köbis et al., 2021; Pehlivanoglu et al., 2026). Conversely, detection systems might be improved by explicitly accounting for these differential vulnerabilities, perhaps through ensemble approaches that weight human and AI detectors contributions based on content characteristics such as pose, noise, and scene complexity (Groh et al., 2021; Ibsen et al., 2024; Josephs et al., 2023).

Confidence calibration and metacognition. Our examination of confidence and accuracy revealed that humans possess genuine metacognitive insight into their detection performance. They were substantially more confident on correct predictions than incorrect ones, aligning with prior work showing that confidence carries useful information about correctness even when absolute calibration is imperfect (Köbis et al., 2021; Janssen et al., 2024; Chen and Goh, 2025; Jin et al., 2025). AI detectors showed much weaker confidence discrimination, meaning their confidence scores carried less diagnostic information about prediction-level correctness, echoing broader concerns that detector scores can be poorly calibrated under distribution shift (Hasan et al., 2026; Xu et al., 2025).

Both groups exhibited a shared asymmetric calibration pattern: overconfidence when predicting a video was real, underconfidence when predicting a deepfake. This asymmetry may reflect prior expectations about base rates of authentic versus fabricated content, or differential difficulty in the two classification directions. Regardless of mechanism, this pattern suggests that both human and AI detectors’ decision thresholds might benefit from recalibration, potentially shifting toward greater skepticism about authenticity in high-stakes settings.

The emergence of the Dunning–Kruger effect in both humans and AI detectors was an unexpected finding. Poor performers systematically overestimated their ability relative to top performers, a pattern that has been documented for humans in related AI-media tasks (Miller et al., 2023; Cooke et al., 2025; Jin et al., 2025) and here appears more pronounced in AI detectors than humans. For AI detectors, this phenomenon likely reflects training dynamics that produce overconfident predictions on out-of-distribution samples (Hasan et al., 2026; Xu et al., 2025). For humans, it suggests that deepfake detection skill may be difficult to introspect—those who lack it may not recognize their deficiency, consistent with prior findings of overconfidence and miscalibration in deepfake detection (Köbis et al., 2021; Chen and Goh, 2025; Casu et al., 2025).

The limited role of demographics. Contrary to common assumptions, demographic factors explained little variance in human detection accuracy. Age, gender, self-reported tech savviness, social media usage frequency, and even self-reported familiarity with deepfakes did not significantly predict performance. This is broadly consistent with prior work finding only small-to-moderate effects of age, experience, and literacy on detection ability (Frank et al., 2023; Müller et al., 2021; Alsobeh et al., 2024; Xie, 2025), and with evidence that more specialized traits (e.g., analytic thinking, visual literacy, or face-recognition aptitude) are more predictive than coarse demographics (Pehlivanoglu et al., 2026; Mink et al., 2024; Davis et al., 2025; Jin et al., 2025).

These findings have implications for training and intervention design. If standard demographic characteristics and self-reported experience do not predict detection ability, interventions may need to focus on developing specific perceptual and cognitive skills rather than simply raising awareness (Tahir et al., 2021). The disconnect between self-reported confidence and actual performance further underscores that people lack insight into their own detection capabilities, suggesting that feedback-based, performance-contingent training approaches might be particularly valuable (Köbis et al., 2021; Chen and Goh, 2025; Jin et al., 2025).

3.1 LIMITATIONS AND FUTURE DIRECTIONS

Several limitations warrant consideration. First, while we evaluated 95 AI detectors variants trained on three datasets, the machine learning landscape changes rapidly, and newer architectures or training strategies might narrow the human-AI performance gap. However, the fundamental vulnerability to distribution shift that we document is unlikely to be resolved by architectural improvements alone, echoing concerns raised by recent analyses of benchmark shortcut learning and cross-generator failures (Xu et al., 2025; Hasan et al., 2026; Kamali et al., 2025).

Second, our human participants evaluated videos in an experimental context that explicitly primed attention to authenticity. In naturalistic social media environments, where attention is not focused on accuracy, sharing behavior may diverge from discernment ability (Cooke et al., 2025; Frank et al., 2023; Sanchez-Acedo et al., 2024a). Future work should examine how these findings translate to ecological settings where people are browsing, not explicitly evaluating, and where deepfakes are rare, viewing time is limited, and attention is divided (Josephs et al., 2024; Cooke et al., 2025).

Third, our deepfakes were generated using specific techniques represented in the DF40 benchmark and our novel CharadesDF dataset. Hyper-realistic deepfakes produced by professional visual effects artists, or future generations of generative models (e.g., diffusion and NeRF-based systems), may present different challenges for both human and AI detectors (Hasan et al., 2026; Kamali et al., 2025). Similarly, we focused on video deepfakes; audio-only or text-based synthetic content may exhibit different patterns of human-AI complementarity, as suggested by work on audio deepfakes, audiovisual face-voice manipulations, and AI-generated text and images (Müller et al., 2021; Hashmi et al., 2024; Frank et al., 2023; Cooke et al., 2025).

Future research might productively explore several directions suggested by our findings. First, understanding what specific perceptual or cognitive strategies successful human detectors employ could inform both training interventions and machine learning architectures (Tahir et al., 2021; Wöhler et al., 2021; Goh, 2024b; Neo et al., 2025). Second, developing content-aware ensemble methods that dynamically weight human and AI detectors’ contributions based on video characteristics might maximize the complementarity we documented (Groh et al., 2021; Ibsen et al., 2024; Boyd et al., 2023; Josephs et al., 2023; Casu et al., 2025). Third, examining how detection performance changes with video duration, context, base rates, and prior expectations could inform practical deployment strategies (Josephs et al., 2024; Janssen et al., 2024; Cooke et al., 2025; Xie, 2025). Finally, as generative technologies continue to advance, longitudinal studies tracking the evolution of human and AI-based detection capabilities will be essential for maintaining effective defenses against synthetic media threats (Hasan et al., 2026; Jin et al., 2025).

3.2 ETHICAL AND SOCIETAL IMPACT

This research was conducted to advance scientific understanding of human and AI capabilities in detecting synthetic media, with the goal of informing more effective defenses against potential misuse of deepfake technology (Köbis et al., 2021; Appel and Prietzel, 2022; Sanchez-Acedo et al.,

2024a). Our findings suggest that dismissing human judgment in favor of purely automated detection systems may be premature, and that human-in-the-loop approaches may offer the most robust path forward (Groh et al., 2021; Ibsen et al., 2024; Jin et al., 2025).

The demonstration that humans outperform AI detectors on challenging, naturalistic content has direct implications for content moderation practices. Platforms might consider integrating human judgment into detection pipelines rather than relying solely on automated systems, particularly for high-stakes decisions where confident misclassifications carry significant costs (Groh et al., 2021; Ibsen et al., 2024; Sanchez-Acedo et al., 2024a). Our finding that hybrid ensembles eliminate catastrophic failures suggests a specific architectural approach: use AI detectors for initial screening, but route uncertain or high-stakes cases to human review, consistent with proposals in security and identity verification domains (Ibsen et al., 2024; Davis et al., 2025; Godage et al., 2022).

At the same time, several aspects of our findings warrant caution. The documentation of systematic calibration errors in both humans and AI detectors suggests that neither should be trusted unconditionally (Köbis et al., 2021; Miller et al., 2023; Chen and Goh, 2025; Casu et al., 2025). The Dunning–Kruger effect among human detectors implies that confidence should not be taken as a reliable indicator of accuracy (Miller et al., 2023; Cooke et al., 2025; Jin et al., 2025). And the limited role of demographics in predicting performance suggests that simply selecting for particular background characteristics will not guarantee detection competence (Frank et al., 2023; Alsobeh et al., 2024; Xie, 2025).

We note potential dual-use concerns with detailed findings about what makes deepfakes detectable. Understanding that AI detectors rely on low-level statistical properties could inform adversarial strategies to evade detection (Xu et al., 2025; Hasan et al., 2026; Kamali et al., 2025). We have attempted to balance scientific transparency with responsibility by reporting findings at a level that informs defensive applications without providing a detailed roadmap for evasion. We encourage future work in this area to similarly consider the implications of detailed vulnerability disclosure (Sanchez-Acedo et al., 2024a;b).

Finally, our research underscores that deepfake detection is not purely a technical problem. Human perception, cognition, and social context all play important roles in determining how synthetic media is perceived and acted upon (Köbis et al., 2021; Appel and Prietzel, 2022; Preu et al., 2022; Cooke et al., 2025; Frank et al., 2023). Effective responses will likely require not only improved detection technologies but also media literacy education, platform design interventions, and policy frameworks that account for the fundamentally sociotechnical nature of the challenge (Sanchez-Acedo et al., 2024a; Goh, 2024a;b; Sanchez-Acedo et al., 2024b).

4 METHODS

4.1 CONSENT AND ETHICS

This research complied with all relevant ethical regulations and was approved by Northwestern University’s Institutional Review Board (IRB) as a minimal-risk study under the title “Understanding the Impact of Face Clarity and Scene Dynamism on Deepfake Generation Quality and Human Detection Performance” (IRB ID: STU00224530). The study comprised two phases, each governed by separate consent procedures.

In Phase 1 (video generation for CharadesDF), participants were presented with an informed consent statement describing the study’s purpose, the requirement to record videos of themselves, and the potential public release of the resulting dataset for non-commercial academic use. Participants acknowledged the inherent privacy risk that their facial images could be identifying despite the removal of direct identifiers (names, email addresses). In Phase 2 (detection evaluation), participants in both the DF40 and CharadesDF studies were presented with a separate informed consent statement explaining that they would view and evaluate videos containing both authentic recordings and synthetic deepfake versions. Both consent forms described the principal investigator, potential benefits and risks, data handling procedures, and participants’ right to withdraw at any time without penalty. Consent was obtained via checkbox agreement on Qualtrics; a waiver of physical signature was granted by the IRB given the online nature of the study. Participants were provided a link to download a PDF copy of their consent form for their records.

All participants were compensated at a rate of \$10 for approximately one hour of participation. Compensation was contingent on completing the study. Participants found to be ineligible after starting were not compensated, and repeat participation was not permitted.

4.2 DIGITAL EXPERIMENT INTERFACE

Both detection experiments (Phase 2) were hosted on Qualtrics. Participants first completed a demographic and background questionnaire, then viewed and evaluated 60 videos presented in randomized order. Each video lasted around 30 seconds. For each video, participants were asked to rate their confidence that the video was authentic using a 5-point Likert scale (1 = “Definitely a Deepfake,” 2 = “Likely a Deepfake,” 3 = “Unsure,” 4 = “Likely Authentic,” 5 = “Definitely Authentic”). We converted these ordinal responses to continuous probability scores $p \in [0, 1]$, where $p = 1$ indicates maximum confidence that the video is a deepfake. Specifically, Likert responses of 1 through 5 were mapped to probability scores of 1.0, 0.75, 0.5, 0.25, and 0.0, respectively.

4.3 EXPERIMENT STIMULI

DF40 dataset. The DF40 dataset Yan et al. (2024b) is a large-scale, comprehensive benchmark for deepfake detection that substantially extends prior datasets in both diversity and scale. From its held-out test set, we sampled 500 fake videos uniformly at random across 10 forgery techniques spanning two categories of face manipulation: face-swapping methods (FSGAN Nirkin et al. (2019), FaceSwap Kowalski (n.d.), SimSwap Chen et al. (2021a), InSwapper Wang (2023), Blend-Face Shiohara et al. (2023), UniFace Xu et al. (2022a), MobileFaceSwap Xu et al. (2022b)) and face-reenactment methods (Wav2Lip Prajwal et al. (2020), HyperReenact Bounareli et al. (2023), SadTalker Zhang et al. (2023)). These 500 fake videos were balanced with 500 real videos sourced from the original YouTube content in FaceForensics++ Rössler et al. (2019) (c23 compression) and Celeb-DF Li et al. (2020), yielding 1,000 evaluation stimuli. The DF40 benchmark was designed to address limitations of prior datasets that relied on outdated forgery techniques or limited manipulation diversity. The dataset features subjects in predominantly frontal poses with consistently visible, clearly resolved faces, representing controlled conditions suitable for systematic evaluation of deepfake detection methods.

CharadesDF dataset. The CharadesDF dataset was developed through Phase 1 of our IRB-approved study to simulate more challenging, real-world detection conditions. We recruited 100 participants via the Prolific platform, each of whom recorded five videos lasting around 15–30 seconds following specific scenario instructions designed to systematically vary face clarity and scene dynamism. All the instructions were randomly sourced from the Charades dataset Sigurdsson et al. (2016), a collection of 9,848 crowdsourced videos depicting casual everyday activities performed by 267 individuals in their own homes, annotated with action labels, temporal intervals, and object classes. Scenarios included activities such as speaking directly to the camera, drinking from a mug, moving around a room while speaking, and presenting in front of a microphone. In our study, each participant also provided one high-quality reference photograph of themselves with clear frontal lighting, which served as the source face for controlled face-swapping experiments.

Using this authentic video dataset of 500 recordings and reference faces, we generated corresponding deepfakes using FaceFusion (v3.2.0)¹, a publicly available face-swapping tool that visually imposes the face of one subject onto the video of another. We selected FaceFusion to emulate the realistic scenario in which individuals without technical backgrounds use publicly available graphical interfaces to create deepfakes without coding skills. To capture a diverse range of synthetic artifacts, we employed five face-swapping models from FaceFusion’s available options: `face_swapper_hyperswap_1a_256` (the default), `inswapper_128_fp16` (the fastest), `hififace_unofficial_256` (the highest quality), `inswapper_128` (a popular user choice), and `blend_swap` (an older, lower-quality model). These models were chosen to represent variation in popularity, speed, output quality, and software evolution. Each model was applied to 100 videos, yielding 500 deepfakes. Combined with the 500 authentic recordings, this produced 1,000 evaluation stimuli. The CharadesDF dataset exhibits substantially greater variability than DF40 in

¹<https://facefusion.io>

image quality, camera angles, and face visibility, including partial occlusions and profile views, reflecting the diversity of conditions encountered in real-world video content.

4.4 PARTICIPANTS

Phase 1: Video generation (CharadesDF). In Phase 1, we recruited 100 participants from the United States via the Prolific platform. Eligibility criteria required participants to be at least 18 years of age, reside in the United States, have access to a device capable of recording video, and consent to the potential public release of their recordings for non-commercial academic use. Each participant recorded five videos and provided one reference photograph, yielding 500 authentic videos. Participants were compensated \$10 for approximately one hour of effort.

Phase 2: Detection evaluation. We conducted two independent detection studies—one using stimuli from DF40 and one using stimuli from CharadesDF—each with 100 participants recruited via Prolific. Eligibility criteria required participants to be at least 18 years of age, reside in the United States, and have access to a device capable of displaying video with adequate screen resolution and audio. Participants who took part in Phase 1 were excluded from Phase 2 to prevent familiarity bias. Due to practical constraints on participant time, each participant viewed a randomly sampled subset of 60 videos from the corresponding 1,000-video dataset such that each video was evaluated by multiple independent raters. Participants were compensated \$10 for approximately one hour of effort.

Prior to viewing the videos, participants completed a background questionnaire that collected demographic information including age, gender, education level, self-reported technology savviness, social media usage frequency, familiarity with deepfake technology, prior exposure to deepfake content, and self-reported confidence in their ability to detect deepfakes.

Table 4 presents the demographic composition of human participants across both datasets. Participants were predominantly aged 25–54 years (DF40: 80%; CharadesDF: 80%), with relatively few participants under 25 or over 65. Gender distribution was approximately balanced (DF40: 47% male, 52% female; CharadesDF: 54% male, 46% female), with no non-binary participants in either sample. Educational attainment was high: the majority held at least a bachelor’s degree (DF40: 59%; CharadesDF: 56%). Most participants rated themselves as average or above average in tech savviness (DF40: 98%; CharadesDF: 98%) and reported daily or more frequent social media usage (DF40: 88%; CharadesDF: 80%). Participants generally reported high familiarity with deepfakes (very or extremely familiar—DF40: 76%; CharadesDF: 61%) and prior exposure to deepfake content (probably or definitely yes—DF40: 86%; CharadesDF: 76%). Self-reported confidence in detection ability was moderate, with most participants indicating they were moderately or very confident (DF40: 70%; CharadesDF: 60%). The demographic similarity across datasets supports the comparability of findings, while the overall sample characteristics suggest a relatively tech-savvy, educated population with substantial self-reported awareness of deepfakes.

4.5 RANDOMIZATION

In both detection experiments, the order of video presentation was fully randomized for each participant. Each participant encountered each video at most once. In the DF40 study, each participant viewed 60 videos randomly sampled from the pool of 1,000 (500 real, 500 fake). In the CharadesDF study, each participant likewise viewed 60 videos randomly sampled from the corresponding pool of 1,000 videos. This randomization ensured that each video received multiple independent ratings while controlling for order effects.

4.6 QUALITY FEATURES EXTRACTION

To examine how visual quality characteristics influence detection performance, we extracted 20 quality features from each video using a two-stage pipeline. We first applied face alignment and cropping using dlib’s frontal face detector with 81-point landmark prediction, following the preprocessing protocol from DeepfakeBench Yan et al. (2023b)². Faces were aligned using a similarity

²<https://github.com/SCLBD/DeepfakeBench/blob/main/preprocessing/preprocess.py>

Table 4: Participant demographics summary.

Variable	Category	DF40	CharadesDF
Age	Under 18	0 (0.0%)	0 (0.0%)
	18–24 years old	5 (5.0%)	2 (2.0%)
	25–34 years old	38 (38.0%)	33 (33.0%)
	35–44 years old	28 (28.0%)	23 (23.0%)
	45–54 years old	14 (14.0%)	24 (24.0%)
	55–64 years old	10 (10.0%)	12 (12.0%)
	65+ years old	5 (5.0%)	6 (6.0%)
Gender	Male	47 (47.0%)	54 (54.0%)
	Female	52 (52.0%)	46 (46.0%)
	Non-binary / third gender	0 (0.0%)	0 (0.0%)
Education	Some high school or less	1 (1.0%)	0 (0.0%)
	High school diploma or GED	16 (16.0%)	15 (15.0%)
	Some college, but no degree	14 (14.0%)	21 (21.0%)
	Associates or technical degree	9 (9.0%)	8 (8.0%)
	Bachelor’s degree	38 (38.0%)	32 (32.0%)
	Graduate or professional degree	21 (21.0%)	24 (24.0%)
Tech Savviness	Beginner	0 (0.0%)	0 (0.0%)
	Below average	2 (2.0%)	2 (2.0%)
	Average	32 (32.0%)	40 (40.0%)
	Above average	57 (57.0%)	42 (42.0%)
	Expert	9 (9.0%)	16 (16.0%)
Social Media Usage	Never	0 (0.0%)	2 (2.0%)
	Rarely (less than once a week)	3 (3.0%)	1 (1.0%)
	Sometimes (1–3 times per week)	6 (6.0%)	3 (3.0%)
	Often (4–6 times per week)	3 (3.0%)	14 (14.0%)
	Daily	37 (37.0%)	31 (31.0%)
	Multiple times per day	51 (51.0%)	49 (49.0%)
Deepfake Familiarity	Not familiar at all	3 (3.0%)	4 (4.0%)
	Slightly familiar	5 (5.0%)	9 (9.0%)
	Moderately familiar	16 (16.0%)	26 (26.0%)
	Very familiar	50 (50.0%)	33 (33.0%)
	Extremely familiar	26 (26.0%)	28 (28.0%)
Prior Deepfake Exposure	Definitely not	4 (4.0%)	10 (10.0%)
	Probably not	2 (2.0%)	7 (7.0%)
	Might or might not	8 (8.0%)	7 (7.0%)
	Probably yes	30 (30.0%)	26 (26.0%)
	Definitely yes	56 (56.0%)	50 (50.0%)
Self-Reported Confidence	Not confident at all	4 (4.0%)	1 (1.0%)
	Slightly confident	17 (17.0%)	30 (30.0%)
	Moderately confident	46 (46.0%)	37 (37.0%)
	Very confident	24 (24.0%)	23 (23.0%)
	Extremely confident	9 (9.0%)	9 (9.0%)
Total	<i>N</i>	100	100

transformation based on five key facial landmarks (left eye, right eye, nose tip, left mouth corner, right mouth corner) and resized to 256×256 pixels. Videos without detectable faces in all sampled frames were excluded, yielding 997 videos in DF40 and 779 in CharadesDF.

Quality features were extracted at the frame level and aggregated to video-level statistics using the mean across all frames containing detected faces. We used two complementary extraction approaches: (1) geometric and photometric features computed directly from facial landmarks and image statistics on the original, unprocessed frames, and (2) semantic quality factors derived from CLIB-FIQA Ou et al. (2024), a vision-language model trained to assess face image quality through joint learning with multiple quality factors, applied to the preprocessed and aligned face crops.

Table 5 provides detailed descriptions of all extracted features. Features were standardized (zero mean, unit variance) within each dataset prior to regression analysis.

Distributional differences between DF40 and CharadesDF. We conducted Mann-Whitney U tests with the Benjamini-Hochberg false discovery rate correction to compare quality feature distributions between DF40 and CharadesDF (Table 6). Consistent with our design goals, CharadesDF exhibited significantly lower visual quality across multiple dimensions. Overall quality scores were substantially lower in CharadesDF ($\mu = 0.596$, Mdn = 0.609) compared to DF40 ($\mu = 0.676$, Mdn = 0.679), $p < 0.001$. Face presence ratio showed the largest absolute difference: DF40 videos contained detectable faces in nearly all frames ($\mu = 1.000$, Mdn = 1.000), whereas CharadesDF videos exhibited substantial frame-to-frame variability in face visibility ($\mu = 0.811$, Mdn = 0.919), reflecting the naturalistic recording conditions where participants moved freely within their environments.

CharadesDF exhibited greater degradation across photometric quality measures: higher blur prevalence (blurry: Mdn = 3.0×10^{-5} vs. 0.0; hazy: Mdn = 1.1×10^{-6} vs. 0.0), lower brightness ($\mu = 89.3$ vs. 112.6), reduced sharpness (Mdn = 40.2 vs. 73.7), and lower contrast ($\mu = 35.7$ vs. 40.4). Pose variability was also greater in CharadesDF, with higher rates of profile views (Mdn = 0.001 vs. 4.2×10^{-6}) and increased occlusion (Mdn = 8.8×10^{-6} vs. 1.8×10^{-7}). These distributional differences confirm that CharadesDF presents substantially more challenging detection conditions than the controlled DF40 benchmark.

Interestingly, DF40 exhibited higher color balance values ($\mu = 25.3$ vs. 18.5), indicating greater color cast variability, and higher mouth aspect ratios ($\mu = 0.891$ vs. 0.827), potentially reflecting the prevalence of lip-sync deepfake methods in that benchmark. Signal-to-noise ratio was marginally higher in CharadesDF (Mdn = 38.6 vs. 34.3), though both datasets showed high variability in this measure. All comparisons reached statistical significance after FDR correction ($p_{\text{FDR}} < 0.05$), underscoring the systematic differences in recording conditions between the controlled YouTube-sourced videos in DF40 and the naturalistic home recordings in CharadesDF.

Table 7 illustrates these quality features with representative frames from both datasets.

Table 5: Quality features extracted for each video. Features are computed per-frame and aggregated to video-level statistics using the mean across frames with detected faces.

Feature	Description
<i>Face Detection and Recognition</i>	
FR Confidence	Face detection confidence score from DeepFace Serengil and Ozpinar (2024), reflecting how reliably the face was detected and localized. Higher values indicate clearer, more frontal faces.
Bbox Area (ratio)	Ratio of the face bounding box area to the total frame area, computed as $(w_{\text{bbox}} \times h_{\text{bbox}})/(w_{\text{frame}} \times h_{\text{frame}})$. Larger values indicate more prominent faces in the frame.
Face Presence (ratio)	Proportion of sampled frames in which at least one face was successfully detected.
<i>Facial Geometry</i>	
IOD	Inter-Ocular Distance: Euclidean distance in pixels between the centers of the left and right eyes, computed from 68-point facial landmarks. Serves as a proxy for face scale and distance from camera.
Left EAR	Left Eye Aspect Ratio: ratio of vertical to horizontal eye extent, computed as $(\ p_1 - p_5\ + \ p_2 - p_4\)/(2 \cdot \ p_0 - p_3\)$ where p_0 - p_5 are the six landmarks of the left eye (indices 36-41 in the 68-point model) Soukupova and Cech (2016). Lower values indicate more closed eyes.
Right EAR	Right Eye Aspect Ratio, computed analogously for the right eye (indices 42-47).
MAR	Mouth Aspect Ratio: computed as $(A + B + C)/(2D)$ where A, B, C are vertical distances between inner lip landmark pairs (51-59, 53-57, 49-55) and D is the horizontal mouth width (48-54). Higher values indicate more open mouths.
<i>Photometric Quality</i>	
SNR	Signal-to-Noise Ratio: estimated as the ratio of mean grayscale intensity to noise standard deviation, where noise is computed as the residual after Gaussian blur with a 5×5 kernel. Higher values indicate cleaner images.
Brightness	Mean pixel intensity of the grayscale-converted face region, ranging from 0 (black) to 255 (white).
Sharpness	Variance of the Laplacian operator applied to the grayscale face region. Higher values indicate sharper images with more high-frequency detail.
Contrast	Standard deviation of pixel intensities in the grayscale face region. Higher values indicate greater tonal range.
Color Balance	Standard deviation across mean R, G, B channel intensities, computed as $\text{std}([\bar{R}, \bar{G}, \bar{B}])$. Lower values indicate more neutral color balance; higher values indicate color casts.
<i>CLIB-FIQA Semantic Factors</i> Ou et al. (2024)	
Blur (blurry)	Probability that the face image is blurry, predicted by CLIB-FIQA. Based on CPBD metric thresholds Narvekar and Karam (2011): scores < 0.35 indicate hazy, 0.35 - 0.7 indicate blurry, > 0.7 indicate clear.
Blur (hazy)	Probability that the face image exhibits haze or fog artifacts (CPBD score < 0.35).
Pose (profile)	Probability that the face is in profile view (yaw angle > 25), classified using Euler angle estimation from facial landmarks.
Pose (slight angle)	Probability that the face is at a slight angle (10 - 25 yaw), intermediate between frontal and profile.
Occlusion	Probability that the face is partially occluded (e.g., by hands, objects, hair, or accessories), predicted by a CNN classifier trained on WiderFace Yang et al. (2016).
Exaggerated Expression	Probability that the face displays an exaggerated or atypical expression (as opposed to neutral or typical expressions), predicted by a CNN classifier.
Extreme Lighting	Probability that the face is under extreme lighting conditions (e.g., harsh shadows, overexposure, backlighting), predicted by a CNN classifier.
Quality Score	Overall face image quality score from CLIB-FIQA, computed as a weighted combination of quality factor probabilities mapped to a five-level scale (bad, poor, fair, good, perfect).

Table 6: Distributional comparison of quality features between DF40 and CharadesDF datasets. Mann-Whitney U tests with Benjamini-Hochberg FDR correction.

Quality Feature	DF40 ($N = 997$)			CharadesDF ($N = 779$)			Direction
	Mean	Median	SD	Mean	Median	SD	
<i>Face Detection and Recognition</i>							
FR Confidence	1.000	1.000	0.0006	0.9995	1.000	0.0024	DF40 >***†
Face Presence (ratio)	1.000	1.000	0.0005	0.811	0.919	0.235	DF40 >***
Bbox Area (ratio)	0.076	0.054	0.069	0.078	0.052	0.081	DF40 >***
<i>Facial Geometry</i>							
IOD	77.08	56.37	47.25	81.40	66.72	61.38	DF40 <*
Left EAR	0.291	0.291	0.033	0.306	0.280	0.106	DF40 >***
Right EAR	0.278	0.282	0.031	0.303	0.271	0.126	DF40 >***
MAR	0.891	0.891	0.083	0.827	0.793	0.172	DF40 >***
<i>Photometric Quality</i>							
SNR	44.55	34.30	32.41	45.24	38.57	27.07	DF40 <***
Brightness	112.64	110.72	22.31	89.29	91.17	26.73	DF40 >***
Sharpness	110.02	73.75	109.78	73.82	40.16	99.14	DF40 >***
Contrast	40.40	39.38	10.51	35.71	36.18	10.90	DF40 >***
Color Balance	25.31	24.93	7.34	18.52	18.83	7.56	DF40 >***
<i>CLIB-FIQA Semantic Factors</i> Ou et al. (2024)							
Blur (blurry)	0.126	0.000	0.323	0.294	3.0×10^{-5}	0.428	DF40 <***
Blur (hazy)	0.001	0.000	0.012	0.280	1.1×10^{-6}	0.436	DF40 <***
Pose (profile)	0.014	4.2×10^{-6}	0.097	0.138	0.001	0.285	DF40 <***
Pose (slight angle)	0.251	0.003	0.393	0.137	0.003	0.270	DF40 >***
Occlusion	0.001	1.8×10^{-7}	0.032	0.058	8.8×10^{-6}	0.203	DF40 <***
Exaggerated expression	0.000	0.000	0.000	3.8×10^{-10}	0.000	1.1×10^{-8}	DF40 <***†
Extreme lighting	0.008	0.000	0.081	0.035	1.8×10^{-7}	0.164	DF40 <***
Quality Score	0.676	0.679	0.038	0.596	0.609	0.091	DF40 >***

Notes: All comparisons significant after Benjamini-Hochberg FDR correction. * $p_{\text{FDR}} < 0.05$, ** $p_{\text{FDR}} < 0.01$, *** $p_{\text{FDR}} < 0.001$. Direction indicates which dataset has higher median values. †Medians are equal; direction based on mean comparison. The Mann-Whitney U test detects significant distributional differences (e.g., in variance or tail behavior) even when medians coincide.

Table 7: Sampled frames from example video stimuli and their associated quality factor values.

	DF40			CharadesDF		
						
	(a)	(b)	(c)	(d)	(e)	(f)
FR Confidence	1.000	1.000	1.000	0.996	1.000	0.995
Bbox Area (ratio)	0.062	0.054	0.052	0.010	0.146	0.241
Face Presence (ratio)	1.00	1.00	1.00	0.769	1.00	0.541
IOD	53.931	131.245	50.110	28.668	135.385	60.197
Left EAR	0.255	0.261	0.289	0.317	0.294	0.396
Right EAR	0.280	0.263	0.266	0.347	0.266	0.292
MAR	0.807	0.804	0.768	0.909	0.865	1.093
SNR	39.091	34.501	40.326	25.063	141.181	33.403
Brightness	129.579	108.013	112.577	53.813	119.192	42.627
Sharpness	79.671	89.321	53.663	167.868	9.040	32.407
Contrast	25.070	28.262	39.507	27.422	32.592	26.575
Color Balance	23.422	30.292	25.352	12.479	29.534	21.420
Blur (blurry)	0.000	0.000	0.000	0.239	0.541	0.133
Blur (hazy)	0.000	0.000	0.000	0.761	0.045	0.866
Pose (profile)	0.000	0.000	0.000	0.242	0.195	0.000
Pose (slight angle)	0.000	0.000	0.000	0.172	0.440	0.506
Occlusion	0.000	0.000	0.000	0.615	0.022	0.001
Exag. Expression	0.000	0.000	0.000	0.000	0.000	0.000
Extreme Lighting	0.000	0.000	0.000	0.000	0.000	0.012
Quality Score	0.664	0.728	0.704	0.526	0.628	0.639

Notes: Each column shows video-level quality factor values for one stimulus. The images above are representative frames sampled from the corresponding video. Values are computed as per-video aggregates. † indicates higher is better; ‡ indicates lower is better; — indicates no direct quality relationship.

4.7 AI DETECTORS

We trained 32 state-of-the-art deepfake detection architectures on three established training datasets: FaceForensics++ Rössler et al. (2019), CelebDF-v2 Li et al. (2020), and the DF40 training split Yan et al. (2024b). This procedure yielded 96 detector variants, with one entry excluded due to architectural incompatibility: the LSDA detector Yan et al. (2024a) could not be trained on CelebDF-v2 because its architecture requires multiple forgery types during training (specifically, four distinct manipulation methods plus real videos) to learn domain-specific encoders and perform latent space augmentation, whereas CelebDF-v2 contains only a single forgery type. Each remaining detector variant was evaluated on all 1,000 videos in both the held-out DF40 test sample and the CharadesDF dataset. No overlap exists between training and evaluation data for any detector variant.

The evaluated architectures span diverse detection paradigms, including frequency-based methods (F3Net Qian et al. (2020), SPSL Liu et al. (2021), SRM Luo et al. (2021)), attention mechanisms (Multi-Attention Zhao et al. (2021a), FFD Dang et al. (2020)), reconstruction-based approaches (RECCE Cao et al. (2022)), contrastive learning (UCF Yan et al. (2023a), PCL-I2G Zhao et al. (2021b)), transformer architectures (UIA-ViT Zhuang et al. (2022), TimeSformer Bertasius et al. (2021)), video-level temporal modeling (I3D Carreira and Zisserman (2017), STIL Gu et al. (2021), VideoMAE Tong et al. (2022)), and foundation model adaptations (CLIP Radford et al. (2021), X-CLIP Ni et al. (2022a)). Backbone architectures included EfficientNet-B4 Tan and Le (2019), Xception Rössler et al. (2019), and various ResNet variants. All models were trained following the protocols specified in DeepfakeBench Yan et al. (2023b) with regards to preprocessing, data augmentation, and optimization hyperparameters within each training dataset condition.

Each detector produced a continuous probability score $p \in [0, 1]$ for each frame, where higher values indicate greater confidence that the frame depicts a deepfake. Frame-level scores were aggregated to video-level predictions by computing the median score across all frames. This aggregation strategy is appropriate for our evaluation setting, where manipulations span the entire video duration; in real-world scenarios where only a subset of frames may be manipulated, alternative aggregation methods—such as maximum pooling or top- k averaging—would be more suitable to avoid diluting localized forgery signals. Binary predictions were obtained by thresholding the aggregated video-level score at $p = 0.5$, consistent with the human evaluation protocol. Tables 8–10 report performance metrics (Accuracy, AUC, F1) for all detector–dataset combinations, with missing entries for LSDA on CelebDF-v2 reflecting the architectural incompatibility described above.

5 DATA AVAILABILITY

The DF40 dataset is publicly available from the original authors at <https://github.com/YZY-stack/DF40>. The CharadesDF dataset, including all 500 authentic home recordings and 500 corresponding deepfakes, will be made publicly available for non-commercial academic use upon publication. The original Charades dataset from which activity instructions were sourced is available at <https://prior.allenai.org/projects/charades>.

6 CODE AVAILABILITY

All code for reproducing the analyses reported in this paper, including scripts for quality feature extraction, ensemble aggregation, statistical analyses, and figure generation, will be made publicly available upon publication. AI detectors were trained using the DeepfakeBench framework (<https://github.com/SCLBD/DeepfakeBench>). Deepfakes for the CharadesDF dataset were generated using FaceFusion v3.2.0 (<https://facefusion.io>). Face quality assessment was performed using CLIB-FIQA (<https://github.com/oufuzhao/CLIB-FIQA>). All additional dependencies and environment specifications are documented in the code repository.

Table 8: Performance (Accuracy) of deepfake detectors trained on FaceForensics++ (FF++), CelebDF-v2 (CDF), or DF40, and evaluated on our DF40 test sample and CharadesDF. Row and column averages are italicized.

Model	Trained on FF++		Trained on CDF		Trained on DF40		Avg
	DF40	CharadesDF	DF40	CharadesDF	DF40	CharadesDF	
Capsule Nguyen et al. (2019)	0.562	0.519	0.558	0.492	0.884	0.553	<i>0.595</i>
CLIP Radford et al. (2021)	0.500	0.493	0.501	0.493	0.541	0.515	<i>0.507</i>
CORE Ni et al. (2022b)	0.669	0.548	0.596	0.614	0.889	0.555	<i>0.645</i>
EfficientNet-B4 Tan and Le (2019)	0.503	0.508	0.556	0.567	0.837	0.501	<i>0.579</i>
Effort Yan et al. (2025)	0.648	0.577	0.658	0.601	0.780	0.628	<i>0.649</i>
F3Net Qian et al. (2020)	0.687	0.547	0.586	0.576	0.916	0.542	<i>0.642</i>
FFD Dang et al. (2020)	0.679	0.597	0.591	0.554	0.934	0.520	<i>0.646</i>
DSP-FWA Li and Lyu (2019)	0.511	0.501	0.378	0.417	0.500	0.510	<i>0.470</i>
I3D Carreira and Zisserman (2017)	0.457	0.518	0.536	0.516	0.501	0.531	<i>0.510</i>
IID Huang et al. (2023)	0.607	0.585	0.533	0.520	0.589	0.519	<i>0.559</i>
Local-relation Chen et al. (2021b)	0.500	0.493	0.500	0.493	0.500	0.507	<i>0.499</i>
LSDA Yan et al. (2024a)	0.508	0.509	—	—	0.614	0.565	<i>0.549</i>
MesoNet Afchar et al. (2018)	0.500	0.493	0.526	0.509	0.500	0.507	<i>0.506</i>
MesoInception Afchar et al. (2018)	0.504	0.516	0.586	0.601	0.645	0.510	<i>0.560</i>
Multi-Attention Zhao et al. (2021a)	0.580	0.493	0.591	0.521	0.603	0.493	<i>0.547</i>
PCL-I2G Zhao et al. (2021b)	0.504	0.507	0.530	0.585	0.504	0.507	<i>0.523</i>
RECCE Cao et al. (2022)	0.675	0.578	0.586	0.561	0.918	0.565	<i>0.647</i>
CNN-Aug Wang et al. (2020)	0.538	0.528	0.587	0.584	0.841	0.568	<i>0.608</i>
RFM Wang and Deng (2021)	0.520	0.539	0.579	0.527	0.905	0.536	<i>0.601</i>
SBI Shiohara and Yamasaki (2022)	0.533	0.469	0.496	0.453	0.515	0.482	<i>0.492</i>
SIA Sun et al. (2022)	0.498	0.530	0.536	0.542	0.707	0.493	<i>0.551</i>
SLADD Chen et al. (2022)	0.732	0.549	0.493	0.490	0.730	0.499	<i>0.582</i>
SPSL Liu et al. (2021)	0.793	0.601	0.601	0.602	0.931	0.525	<i>0.675</i>
SRM Luo et al. (2021)	0.712	0.584	0.588	0.589	0.870	0.554	<i>0.649</i>
STIL Gu et al. (2021)	0.550	0.522	0.607	0.544	0.898	0.606	<i>0.621</i>
TALL Xu et al. (2023)	0.366	0.509	0.500	0.505	0.499	0.499	<i>0.480</i>
TimeSformer Bertasius et al. (2021)	0.570	0.518	0.500	0.513	0.607	0.520	<i>0.538</i>
UCF Yan et al. (2023a)	0.733	0.631	0.573	0.583	0.920	0.556	<i>0.666</i>
UIA-ViT Zhuang et al. (2022)	0.679	0.588	0.579	0.583	0.843	0.600	<i>0.645</i>
VideoMAE Tong et al. (2022)	0.459	0.516	0.458	0.516	0.526	0.515	<i>0.498</i>
Xception Rössler et al. (2019)	0.651	0.579	0.609	0.596	0.876	0.548	<i>0.643</i>
X-CLIP Ni et al. (2022a)	0.366	0.509	0.366	0.509	0.499	0.508	<i>0.459</i>
Avg	<i>0.572</i>	<i>0.536</i>	<i>0.545</i>	<i>0.541</i>	<i>0.713</i>	<i>0.532</i>	<i>0.573</i>

Table 9: Performance (AUC) of deepfake detectors trained on FaceForensics++ (FF++), CelebDF-v2 (CDF), or DF40, and evaluated on our DF40 test sample and CharadesDF. Row and column averages are italicized.

Model	Trained on FF++		Trained on CDF		Trained on DF40		Avg
	DF40	CharadesDF	DF40	CharadesDF	DF40	CharadesDF	
Capsule Nguyen et al. (2019)	0.706	0.561	0.619	0.545	0.983	0.643	<i>0.676</i>
CLIP Radford et al. (2021)	0.530	0.545	0.521	0.590	0.551	0.527	<i>0.544</i>
CORE Ni et al. (2022b)	0.768	0.668	0.634	0.635	0.982	0.582	<i>0.712</i>
EfficientNet-B4 Tan and Le (2019)	0.605	0.626	0.584	0.583	0.929	0.520	<i>0.641</i>
Effort Yan et al. (2025)	0.821	0.753	0.721	0.674	0.953	0.709	<i>0.772</i>
F3Net Qian et al. (2020)	0.768	0.676	0.616	0.635	0.969	0.577	<i>0.707</i>
FFD Dang et al. (2020)	0.825	0.666	0.631	0.623	0.982	0.562	<i>0.715</i>
DSP-FWA Li and Lyu (2019)	0.572	0.586	0.320	0.409	0.465	0.597	<i>0.492</i>
I3D Carreira and Zisserman (2017)	0.533	0.528	0.549	0.531	0.816	0.544	<i>0.583</i>
IID Huang et al. (2023)	0.825	0.634	0.583	0.584	0.834	0.570	<i>0.672</i>
Local-relation Chen et al. (2021b)	0.591	0.608	0.600	0.579	0.495	0.486	<i>0.560</i>
LSDA Yan et al. (2024a)	0.771	0.662	—	—	0.731	0.641	<i>0.701</i>
MesoNet Afchar et al. (2018)	0.623	0.499	0.606	0.564	0.574	0.559	<i>0.571</i>
MesoInception Afchar et al. (2018)	0.607	0.644	0.627	0.623	0.908	0.543	<i>0.659</i>
Multi-Attention Zhao et al. (2021a)	0.432	0.500	0.621	0.606	0.478	0.500	<i>0.523</i>
PCL-I2G Zhao et al. (2021b)	0.535	0.515	0.664	0.650	0.676	0.527	<i>0.595</i>
RECCE Cao et al. (2022)	0.819	0.690	0.622	0.609	0.978	0.594	<i>0.719</i>
CNN-Aug Wang et al. (2020)	0.723	0.611	0.622	0.656	0.958	0.637	<i>0.701</i>
RFM Wang and Deng (2021)	0.765	0.639	0.624	0.566	0.971	0.586	<i>0.692</i>
SBI Shiohara and Yamasaki (2022)	0.537	0.456	0.513	0.436	0.510	0.403	<i>0.476</i>
SIA Sun et al. (2022)	0.537	0.606	0.556	0.558	0.891	0.496	<i>0.607</i>
SLADD Chen et al. (2022)	0.852	0.700	0.492	0.492	0.979	0.588	<i>0.684</i>
SPSL Liu et al. (2021)	0.867	0.634	0.647	0.631	0.983	0.546	<i>0.718</i>
SRM Luo et al. (2021)	0.804	0.662	0.633	0.616	0.982	0.605	<i>0.717</i>
STIL Gu et al. (2021)	0.816	0.594	0.671	0.582	0.971	0.627	<i>0.710</i>
TALL Xu et al. (2023)	0.385	0.504	0.527	0.484	0.630	0.562	<i>0.515</i>
TimeSformer Bertasius et al. (2021)	0.579	0.526	0.542	0.554	0.641	0.528	<i>0.562</i>
UCF Yan et al. (2023a)	0.801	0.691	0.616	0.599	0.982	0.585	<i>0.712</i>
UIA-ViT Zhuang et al. (2022)	0.769	0.692	0.617	0.608	0.946	0.621	<i>0.709</i>
VideoMAE Tong et al. (2022)	0.507	0.527	0.489	0.523	0.535	0.522	<i>0.517</i>
Xception Rössler et al. (2019)	0.818	0.681	0.652	0.639	0.958	0.585	<i>0.722</i>
X-CLIP Ni et al. (2022a)	0.386	0.509	0.399	0.512	0.357	0.506	<i>0.445</i>
Avg	<i>0.671</i>	<i>0.606</i>	<i>0.585</i>	<i>0.577</i>	<i>0.800</i>	<i>0.565</i>	<i>0.635</i>

Table 10: Performance (F1 score) of deepfake detectors trained on FaceForensics++ (FF++), CelebDF-v2 (CDF), or DF40, and evaluated on our DF40 test sample and CharadesDF. Row and column averages are italicized.

Model	Trained on FF++		Trained on CDF		Trained on DF40		Avg
	DF40	CharadesDF	DF40	CharadesDF	DF40	CharadesDF	
Capsule Nguyen et al. (2019)	0.681	0.665	0.629	0.635	0.895	0.674	<i>0.697</i>
CLIP Radford et al. (2021)	0.667	0.661	0.667	0.661	0.526	0.607	<i>0.631</i>
CORE Ni et al. (2022b)	0.727	0.683	0.553	0.618	0.876	0.597	<i>0.676</i>
EfficientNet-B4 Tan and Le (2019)	0.668	0.666	0.534	0.620	0.848	0.568	<i>0.650</i>
Effort Yan et al. (2025)	0.723	0.688	0.563	0.463	0.719	0.569	<i>0.621</i>
F3Net Qian et al. (2020)	0.722	0.678	0.587	0.649	0.913	0.594	<i>0.690</i>
FFD Dang et al. (2020)	0.739	0.690	0.644	0.657	0.933	0.612	<i>0.713</i>
DSP-FWA Li and Lyu (2019)	0.659	0.620	0.421	0.425	0.667	0.663	<i>0.576</i>
I3D Carreira and Zisserman (2017)	0.624	0.519	0.394	0.087	0.643	0.531	<i>0.466</i>
IID Huang et al. (2023)	0.363	0.501	0.168	0.070	0.705	0.660	<i>0.411</i>
Local-relation Chen et al. (2021b)	0.667	0.661	0.667	0.661	0.000	0.000	<i>0.442</i>
LSDA Yan et al. (2024a)	0.668	0.667	—	—	0.695	0.676	<i>0.676</i>
MesoNet Afchar et al. (2018)	0.667	0.661	0.664	0.634	0.000	0.000	<i>0.438</i>
MesoInception Afchar et al. (2018)	0.659	0.667	0.619	0.669	0.451	0.188	<i>0.542</i>
Multi-Attention Zhao et al. (2021a)	0.704	0.661	0.659	0.650	0.716	0.661	<i>0.675</i>
PCL-I2G Zhao et al. (2021b)	0.024	0.000	0.161	0.424	0.024	0.000	<i>0.105</i>
RECCE Cao et al. (2022)	0.732	0.695	0.578	0.637	0.914	0.566	<i>0.687</i>
CNN-Aug Wang et al. (2020)	0.678	0.668	0.603	0.472	0.858	0.672	<i>0.659</i>
RFM Wang and Deng (2021)	0.674	0.676	0.571	0.626	0.907	0.624	<i>0.680</i>
SBI Shiohara and Yamasaki (2022)	0.499	0.148	0.434	0.321	0.490	0.186	<i>0.346</i>
SIA Sun et al. (2022)	0.663	0.673	0.455	0.490	0.609	0.075	<i>0.494</i>
SLADD Chen et al. (2022)	0.763	0.672	0.460	0.470	0.786	0.663	<i>0.636</i>
SPSL Liu et al. (2021)	0.762	0.667	0.529	0.623	0.928	0.602	<i>0.685</i>
SRM Luo et al. (2021)	0.744	0.691	0.586	0.639	0.883	0.682	<i>0.704</i>
STIL Gu et al. (2021)	0.688	0.616	0.452	0.229	0.889	0.552	<i>0.571</i>
TALL Xu et al. (2023)	0.511	0.375	0.667	0.637	0.658	0.629	<i>0.579</i>
TimeSformer Bertasius et al. (2021)	0.609	0.499	0.667	0.611	0.488	0.424	<i>0.550</i>
UCF Yan et al. (2023a)	0.708	0.687	0.446	0.575	0.915	0.624	<i>0.659</i>
UIA-ViT Zhuang et al. (2022)	0.718	0.679	0.499	0.527	0.826	0.579	<i>0.638</i>
VideoMAE Tong et al. (2022)	0.629	0.538	0.628	0.538	0.342	0.134	<i>0.468</i>
Xception Rössler et al. (2019)	0.725	0.690	0.589	0.640	0.867	0.574	<i>0.681</i>
X-CLIP Ni et al. (2022a)	0.511	0.375	0.511	0.375	0.000	0.005	<i>0.296</i>
Avg	<i>0.643</i>	<i>0.595</i>	<i>0.536</i>	<i>0.527</i>	<i>0.655</i>	<i>0.475</i>	<i>0.572</i>

REFERENCES

- Darius Afchar, Vincent Nozick, Junichi Yamagishi, and Isao Echizen. Mesonet: a compact facial video forgery detection network. In *IEEE International Workshop on Information Forensics and Security (WIFS)*, pages 1–7. IEEE, 2018.
- Anas Alsobeh, Alan Franklin, Belle Woodward, M. Porche, and Joseph Siegelman. Unmasking media illusion: Analytical survey of deepfake video detection and emotional insights. *Issues In Information Systems*, 2024. doi: 10.48009/2_iis_2024_108.
- Markus Appel and Fabian Prietzel. The detection of political deepfakes. *Journal of Computer-Mediated Communication*, 27(4):zmac008, 2022.
- Gedas Bertasius, Heng Wang, and Lorenzo Torresani. Is space-time attention all you need for video understanding? In *International Conference on Machine Learning (ICML)*, pages 813–824. PMLR, 2021.
- Stella Bounareli, Christos Tzelepis, Vasileios Argyriou, Ioannis Patras, and Georgios Tzimiropoulos. Hyperreenact: One-shot reenactment via jointly learning to refine and retarget faces. In *IEEE/CVF International Conference on Computer Vision, ICCV 2023, Paris, France, October 1-6, 2023*, pages 7115–7125. IEEE, 2023. doi: 10.1109/ICCV51070.2023.00657. URL <https://doi.org/10.1109/ICCV51070.2023.00657>.
- Aidan Boyd, Patrick Tinsley, Kevin Bowyer, and Adam Czajka. The value of ai guidance in human examination of synthetically-generated faces. In *Proceedings of the AAAI Conference on Artificial Intelligence*, volume 37, pages 5930–5938, 2023.
- Sergi D. Bray, Shane D. Johnson, and Bennett Kleinberg. Testing human ability to detect deepfake images of human faces. *J. Cybersecur.*, 9, 2022. doi: 10.48550/arXiv.2212.05056.
- Junyi Cao, Chao Ma, Taiping Yao, Shen Chen, Shouhong Ding, and Xiaokang Yang. End-to-end reconstruction-classification learning for face forgery detection. In *Proceedings of the IEEE/CVF Conference on Computer Vision and Pattern Recognition (CVPR)*, pages 4113–4122, 2022.
- João Carreira and Andrew Zisserman. Quo vadis, action recognition? a new model and the kinetics dataset. In *Proceedings of the IEEE/CVF Conference on Computer Vision and Pattern Recognition (CVPR)*, pages 6299–6308, 2017.
- Mirko Casu, Luca Guarnera, Ignazio Zangara, P. Caponnetto, and S. Battiato. A (mid)journey through reality: Assessing accuracy, impostor bias, and automation bias in human detection of ai-generated images. *Human Behavior and Emerging Technologies*, 2025. doi: 10.1155/hbe2/9977058.
- Chen Chen and D. Goh. The role of self-efficacy, critical thinking, and media literacy in human deepfake video detection. *Proceedings of the Association for Information Science and Technology*, 62, 2025. doi: 10.1002/pa2.1310.
- Liang Chen, Yong Zhang, Yibing Song, Lingqiao Liu, and Jue Wang. Self-supervised learning of adversarial example: Towards good generalizations for deepfake detection. In *Proceedings of the IEEE/CVF Conference on Computer Vision and Pattern Recognition (CVPR)*, pages 18710–18719, 2022.
- Renwang Chen, Xuanhong Chen, Bingbing Ni, and Yanhao Ge. Simswap: An efficient framework for high fidelity face swapping. *CoRR*, abs/2106.06340, 2021a. URL <https://arxiv.org/abs/2106.06340>.
- Shen Chen, Taiping Yao, Yang Chen, Shouhong Ding, Jilin Li, and Rongrong Ji. Local relation learning for face forgery detection. In *Proceedings of the AAAI Conference on Artificial Intelligence*, volume 35, pages 1081–1088, 2021b.
- Di Cooke, Abigail Edwards, Sophia Barkoff, and Kathryn Kelly. As good as a coin toss: Human detection of ai-generated content. *Communications of the ACM*, 68:100 – 109, 2025. doi: 10.1145/3729417.

-
- Alejandro Cuevas and Manoel Horta Ribeiro. Deepfake pornography is resilient to regulatory and platform shocks. *arXiv preprint arXiv:2602.02754*, 2026.
- Hao Dang, Feng Liu, Joel Stehouwer, Xiaoming Liu, and Anil K Jain. On the detection of digital face manipulation. In *Proceedings of the IEEE/CVF Conference on Computer Vision and Pattern Recognition (CVPR)*, pages 5781–5790, 2020.
- Josh P. Davis, David J. Robertson, Ryan E. Jenkins, M. Ibsen, Robert Nichols, Martha Babbs, C. Rathgeb, Frøy Løvåsdal, Kiran Raja, and Christoph Busch. The super-recogniser advantage extends to the detection of digitally manipulated faces. *Applied Cognitive Psychology*, 2025. doi: 10.1002/acp.70053.
- David Eigen, Christian Puhersch, and Rob Fergus. Depth map prediction from a single image using a multi-scale deep network. In Zoubin Ghahramani, Max Welling, Corinna Cortes, Neil D. Lawrence, and Kilian Q. Weinberger, editors, *Advances in Neural Information Processing Systems 27: Annual Conference on Neural Information Processing Systems 2014, December 8-13 2014, Montreal, Quebec, Canada*, pages 2366–2374, 2014. URL <https://proceedings.neurips.cc/paper/2014/hash/7bccfde7714a1ebadf06c5f4cea752c1-Abstract.html>.
- Joel Frank, Franziska Herbert, Jonas Ricker, L. Schönherr, Thorsten Eisenhofer, Asja Fischer, Markus Dürmuth, and Thorsten Holz. A representative study on human detection of artificially generated media across countries. *2024 IEEE Symposium on Security and Privacy (SP)*, pages 55–73, 2023. doi: 10.1109/SP54263.2024.00159.
- W Brier Glenn et al. Verification of forecasts expressed in terms of probability. *Monthly weather review*, 78(1):1–3, 1950.
- Sankini Ranca Godage, Frøy Løvåsdal, S. Venkatesh, K. Raja, Raghavendra Ramachandra, and C. Busch. Analyzing human observer ability in morphing attack detection—where do we stand? *IEEE Transactions on Technology and Society*, 4:125–145, 2022. doi: 10.1109/TTS.2022.3231450.
- D. Goh. “he looks very real”: Media, knowledge, and search-based strategies for deepfake identification. *Journal of the Association for Information Science and Technology*, 75:643 – 654, 2024a. doi: 10.1002/asi.24867.
- D. Goh. “he looks very real”: Media, knowledge, and search-based strategies for deepfake identification. *Journal of the Association for Information Science and Technology*, 75:643 – 654, 2024b. doi: 10.1002/asi.24867.
- D. Goh, Jonathan Pan, and C. S. Lee. Humans versus machines: A deepfake detection faceoff. *Proceedings of the Association for Information Science and Technology*, 61, 2024. doi: 10.1002/pr2.1139.
- Matthew Groh, Ziv Epstein, C. Firestone, and Rosalind W. Picard. Deepfake detection by human crowds, machines, and machine-informed crowds. *Proceedings of the National Academy of Sciences of the United States of America*, 119, 2021. doi: 10.1073/pnas.2110013119.
- Zhihao Gu, Yang Chen, Taiping Yao, Shouhong Ding, Jilin Li, Feiyue Huang, and Lizhuang Ma. Spatiotemporal inconsistency learning for deepfake video detection. In *Proceedings of the 29th ACM International Conference on Multimedia*, pages 3473–3481, 2021.
- Parul Gupta, Komal Chugh, Abhinav Dhall, and Ramanathan Subramanian. The eyes know it: Fakeet- an eye-tracking database to understand deepfake perception. *Proceedings of the 2020 International Conference on Multimodal Interaction*, 2020. doi: 10.1145/3382507.3418857.
- Md. Tarek Hasan, Sanjay Saha, Shaojing Fan, Swakkhar Shatabda, and Terence Sim. Deepfake synthesis vs. detection: An uneven contest. *Unknown Journal*, 2026.
- Ammarah Hashmi, Sahibzada Adil Shahzad, Chia-Wen Lin, Yu Tsao, and Hsin-Min Wang. Unmasking illusions: Understanding human perception of audiovisual deepfakes. *ArXiv*, abs/2405.04097, 2024. doi: 10.48550/arXiv.2405.04097.

-
- Baojin Huang, Zhongyuan Wang, Jifan Yang, Jiaxin Ai, Qin Zou, Qian Wang, and Dengpan Ye. Implicit identity driven deepfake face swapping detection. In *Proceedings of the IEEE/CVF Conference on Computer Vision and Pattern Recognition (CVPR)*, pages 4490–4499, 2023.
- M. Ibsen, Robert Nichols, C. Rathgeb, David J. Robertson, Josh P. Davis, Frøy Løvåsdal, Kiran Raja, Ryan E. Jenkins, and Christoph Busch. Conditional face image manipulation detection: Combining algorithm and human examiner decisions. *Proceedings of the 2024 ACM Workshop on Information Hiding and Multimedia Security*, 2024. doi: 10.1145/3658664.3659649.
- Eva M. Janssen, Yarno F. Mutis, and Tamara van Gog. Looks real, feels fake: conflict detection in deepfake videos. *Thinking & Reasoning*, 31:237 – 247, 2024. doi: 10.1080/13546783.2024.2391794.
- Xinyi Jin, Guoyan Wang, Zhuoyue Zhang, Wenbo Zhou, Nenghai Yu, Bowen Gao, and Shuqing Gao. Identifying individual differences in deepfake discernment: the effects of cognitive disposition and visual literacy. *Information, Communication & Society*, 28:3066 – 3085, 2025. doi: 10.1080/1369118X.2025.2496902.
- Emilie Josephs, Camilo Luciano Fosco, and A. Oliva. Artifact magnification on deepfake videos increases human detection and subjective confidence. *ArXiv*, abs/2304.04733, 2023. doi: 10.48550/arXiv.2304.04733.
- Emilie Josephs, Camilo Luciano Fosco, and A. Oliva. Effects of browsing conditions and visual alert design on human susceptibility to deepfakes. *Journal of Online Trust and Safety*, 2024. doi: 10.54501/jots.v2i2.144.
- Negar Kamali, Karyn Nakamura, Aakriti Kumar, Angelos Chatzimparmpas, Jessica Hullman, and Matthew Groh. Characterizing photorealism and artifacts in diffusion model-generated images. *Proceedings of the 2025 CHI Conference on Human Factors in Computing Systems*, 2025. doi: 10.1145/3706598.3713962.
- Nils C Köbis, Barbora Doležalová, and Ivan Soraperra. Fooled twice: People cannot detect deepfakes but think they can. *Iscience*, 24(11), 2021.
- Pavel Korshunov and S. Marcel. Subjective and objective evaluation of deepfake videos. *ICASSP 2021 - 2021 IEEE International Conference on Acoustics, Speech and Signal Processing (ICASSP)*, pages 2510–2514, 2021. doi: 10.1109/ICASSP39728.2021.9414258.
- Marek Kowalski. Faceswap: 3d face swapping implemented in python. n.d. GitHub repository, accessed February 2026.
- Yuezun Li and Siwei Lyu. Exposing deepfake videos by detecting face warping artifacts. In *IEEE Conference on Computer Vision and Pattern Recognition Workshops (CVPRW)*, pages 46–52, 2019.
- Yuezun Li, Xin Yang, Pu Sun, Honggang Qi, and Siwei Lyu. Celeb-df: A large-scale challenging dataset for deepfake forensics. In *Proceedings of the IEEE/CVF conference on computer vision and pattern recognition*, pages 3207–3216, 2020.
- Honggu Liu, Xiaodan Li, Wenbo Zhou, Yuefeng Chen, Yuan He, Hui Xue, Weiming Zhang, and Nenghai Yu. Spatial-phase shallow learning: Rethinking face forgery detection in frequency domain. In *Proceedings of the IEEE/CVF Conference on Computer Vision and Pattern Recognition (CVPR)*, pages 772–781, 2021.
- Yuchen Luo, Yong Zhang, Junchi Yan, and Wei Liu. Generalizing face forgery detection with high-frequency features. In *Proceedings of the IEEE/CVF Conference on Computer Vision and Pattern Recognition (CVPR)*, pages 16317–16326, 2021.
- Elizabeth J. Miller, B. A. Steward, Zak Witkower, C. Sutherland, Eva G. Krumhuber, and Amy Dawel. Ai hyperrealism: Why ai faces are perceived as more real than human ones. *Psychological Science*, 34:1390 – 1403, 2023. doi: 10.1177/09567976231207095.

-
- Jaron Mink, Miranda Wei, Collins W. Munyendo, Kurt Hugenberg, Tadayoshi Kohno, Elissa M. Redmiles, and Gang Wang. It's trying too hard to look real: Deepfake moderation mistakes and identity-based bias. *Proceedings of the 2024 CHI Conference on Human Factors in Computing Systems*, 2024. doi: 10.1145/3613904.3641999.
- N. Müller, Karla Markert, and Konstantin Böttinger. Human perception of audio deepfakes. *Proceedings of the 1st International Workshop on Deepfake Detection for Audio Multimedia*, 2021. doi: 10.1145/3552466.3556531.
- Mahdi Pakdaman Naeini, Gregory F. Cooper, and Milos Hauskrecht. Obtaining well calibrated probabilities using bayesian binning. In Blai Bonet and Sven Koenig, editors, *Proceedings of the Twenty-Ninth AAAI Conference on Artificial Intelligence, January 25-30, 2015, Austin, Texas, USA*, pages 2901–2907. AAAI Press, 2015. doi: 10.1609/AAAI.V29I1.9602. URL <https://doi.org/10.1609/aaai.v29i1.9602>.
- Niranjan D Narvekar and Lina J Karam. A no-reference image blur metric based on the cumulative probability of blur detection (cpbd). *IEEE Transactions on Image Processing*, 20(9):2678–2683, 2011.
- Celene Neo, D. Goh, Rachel Wan Ying Chun, and C. S. Lee. Uncovering strategies for identifying deepfakes. *Inf. Res.*, 30:752–760, 2025. doi: 10.47989/ir30iconf47209.
- Huy H Nguyen, Junichi Yamagishi, and Isao Echizen. Capsule-forensics: Using capsule networks to detect forged images and videos. In *IEEE International Conference on Acoustics, Speech and Signal Processing (ICASSP)*, pages 2307–2311. IEEE, 2019.
- Bolin Ni, Houwen Peng, Minghao Chen, Songyang Zhang, Gaofeng Meng, Jianlong Fu, Shiming Xiang, and Haibin Ling. Expanding language-image pretrained models for general video recognition. In *European Conference on Computer Vision (ECCV)*, pages 1–18. Springer, 2022a.
- Yunsheng Ni, Depu Meng, Changqian Yu, Chengbin Quan, Dongchun Ren, and Youjian Zhao. Core: Consistent representation learning for face forgery detection. In *Proceedings of the IEEE/CVF Conference on Computer Vision and Pattern Recognition Workshops (CVPRW)*, pages 12–21, 2022b.
- Robert Nichols, C. Rathgeb, P. Drozdowski, and C. Busch. Psychophysical evaluation of human performance in detecting digital face image manipulations. *IEEE Access*, 10:31359–31376, 2022. doi: 10.1109/ACCESS.2022.3160596.
- Yuval Nirkin, Yosi Keller, and Tal Hassner. FSGAN: subject agnostic face swapping and reenactment. In *2019 IEEE/CVF International Conference on Computer Vision, ICCV 2019, Seoul, Korea (South), October 27 - November 2, 2019*, pages 7183–7192. IEEE, 2019. doi: 10.1109/ICCV.2019.00728. URL <https://doi.org/10.1109/ICCV.2019.00728>.
- Fu-Zhao Ou, Chongyi Li, Shiqi Wang, and Sam Kwong. Clib-fiq: Face image quality assessment with confidence calibration. In *Proceedings of the IEEE/CVF Conference on Computer Vision and Pattern Recognition*, pages 1694–1704, 2024.
- Didem Pehlivanoglu, Mengdi Zhu, Jialong Zhen, Aude A Gagnon-Roberge, Rebecca K Kern, Damon Woodard, Brian S Cahill, and Natalie C Ebner. Is this real? susceptibility to deepfakes in machines and humans. *Cognitive Research: Principles and Implications*, 11, 2026. doi: 10.1186/s41235-025-00700-y.
- K. R. Prajwal, Rudrabha Mukhopadhyay, Vinay P. Namboodiri, and C. V. Jawahar. A lip sync expert is all you need for speech to lip generation in the wild. In Chang Wen Chen, Rita Cucchiara, Xian-Sheng Hua, Guo-Jun Qi, Elisa Ricci, Zhengyou Zhang, and Roger Zimmermann, editors, *MM '20: The 28th ACM International Conference on Multimedia, Virtual Event / Seattle, WA, USA, October 12-16, 2020*, pages 484–492. ACM, 2020. doi: 10.1145/3394171.3413532. URL <https://doi.org/10.1145/3394171.3413532>.
- S. S. Prasad, O. Hadar, Thang Vu, and I. Polian. Human vs. automatic detection of deepfake videos over noisy channels. *2022 IEEE International Conference on Multimedia and Expo (ICME)*, pages 1–6, 2022. doi: 10.1109/ICME52920.2022.9859954.

-
- Ethan Preu, Mark Jackson, and Nazim Choudhury. Perception vs. reality: Understanding and evaluating the impact of synthetic image deepfakes over college students. In *2022 IEEE 13th Annual Ubiquitous Computing, Electronics & Mobile Communication Conference (UEMCON)*, pages 0547–0553. IEEE, 2022.
- Yuyang Qian, Guojun Yin, Lu Sheng, Zixuan Chen, and Jing Shao. Thinking in frequency: Face forgery detection by mining frequency-aware clues. In *European Conference on Computer Vision (ECCV)*, pages 86–103. Springer, 2020.
- Alec Radford, Jong Wook Kim, Chris Hallacy, Aditya Ramesh, Gabriel Goh, Sandhini Agarwal, Girish Sastry, Amanda Askell, Pamela Mishkin, Jack Clark, et al. Learning transferable visual models from natural language supervision. In *International Conference on Machine Learning (ICML)*, pages 8748–8763. PMLR, 2021.
- Andreas Rössler, Davide Cozzolino, Luisa Verdoliva, Christian Riess, Justus Thies, and Matthias Nießner. Faceforensics++: Learning to detect manipulated facial images. In *2019 IEEE/CVF International Conference on Computer Vision, ICCV 2019, Seoul, Korea (South), October 27 - November 2, 2019*, pages 1–11. IEEE, 2019. doi: 10.1109/ICCV.2019.00009. URL <https://doi.org/10.1109/ICCV.2019.00009>.
- Andreas Rössler, Davide Cozzolino, Luisa Verdoliva, Christian Riess, Justus Thies, and Matthias Nießner. Faceforensics++: Learning to detect manipulated facial images. In *Proceedings of the IEEE/CVF International Conference on Computer Vision (ICCV)*, pages 1–11, 2019.
- Alberto Sanchez-Acedo, Alejandro Carbonell-Alcocer, Manuel Gertrudix, and Jose-Luis Rubio-Tamayo. The challenges of media and information literacy in the artificial intelligence ecology: deepfakes and misinformation. *Communication & Society*, pages 223–239, 2024a.
- Alberto Sanchez-Acedo, Alejandro Carbonell-Alcocer, Manuel Gertrudix, and J. Rubio-Tamayo. The challenges of media and information literacy in the artificial intelligence ecology: deepfakes and misinformation. *Communication & Society*, 2024b. doi: 10.15581/003.37.4.223-239.
- Sefik Ilkin Serengil and Alper Ozpinar. A benchmark of facial recognition pipelines and co-usability performances of modules. *Journal of Information Technologies*, 2024.
- Kaede Shiohara and Toshihiko Yamasaki. Detecting deepfakes with self-blended images. In *Proceedings of the IEEE/CVF Conference on Computer Vision and Pattern Recognition (CVPR)*, pages 18720–18729, 2022.
- Kaede Shiohara, Xingchao Yang, and Takafumi Taketomi. Blendface: Re-designing identity encoders for face-swapping. In *IEEE/CVF International Conference on Computer Vision, ICCV 2023, Paris, France, October 1-6, 2023*, pages 7600–7610. IEEE, 2023. doi: 10.1109/ICCV51070.2023.00702. URL <https://doi.org/10.1109/ICCV51070.2023.00702>.
- Gunnar A. Sigurdsson, Gül Varol, Xiaolong Wang, Ali Farhadi, Ivan Laptev, and Abhinav Gupta. Hollywood in homes: Crowdsourcing data collection for activity understanding. In Bastian Leibe, Jiri Matas, Nicu Sebe, and Max Welling, editors, *Computer Vision - ECCV 2016 - 14th European Conference, Amsterdam, The Netherlands, October 11-14, 2016, Proceedings, Part I*, volume 9905 of *Lecture Notes in Computer Science*, pages 510–526. Springer, 2016. doi: 10.1007/978-3-319-46448-0_31. URL https://doi.org/10.1007/978-3-319-46448-0_31.
- Tereza Soukupova and Jan Cech. Eye blink detection using facial landmarks. In *21st Computer Vision Winter Workshop*, 2016.
- Ke Sun, Hong Liu, Qixiang Ye, Yue Gao, Jianzhuang Liu, Ling Shao, and Rongrong Ji. An information theoretic approach for attention-driven face forgery detection. In *European Conference on Computer Vision (ECCV)*, pages 111–127. Springer, 2022.
- Rashid Tahir, Brishna Batool, Hira Jamshed, Mahnoor Jameel, Mubashir Anwar, Faizan Ahmed, M. Zaffar, and Muhammad Fareed Zaffar. Seeing is believing: Exploring perceptual differences in deepfake videos. *Proceedings of the 2021 CHI Conference on Human Factors in Computing Systems*, 2021. doi: 10.1145/3411764.3445699.

-
- Mingxing Tan and Quoc Le. Efficientnet: Rethinking model scaling for convolutional neural networks. In *International Conference on Machine Learning (ICML)*, pages 6105–6114. PMLR, 2019.
- Zhan Tong, Yibing Song, Jue Wang, and Limin Wang. Videomae: Masked autoencoders are data-efficient learners for self-supervised video pre-training. In *Advances in Neural Information Processing Systems (NeurIPS)*, volume 35, pages 10078–10093, 2022.
- Chengrui Wang and Weihong Deng. Representative forgery mining for fake face detection. In *Proceedings of the IEEE/CVF Conference on Computer Vision and Pattern Recognition (CVPR)*, pages 14923–14932, 2021.
- Haofan Wang. Inswapper: One-click face swapper and restoration powered by insightface. 2023. GitHub repository, accessed February 2026.
- Sheng-Yu Wang, Oliver Wang, Richard Zhang, Andrew Owens, and Alexei A Efros. Cnn-generated images are surprisingly easy to spot... for now. In *Proceedings of the IEEE/CVF Conference on Computer Vision and Pattern Recognition (CVPR)*, pages 8695–8704, 2020.
- L. Wöhler, Susana Castillo, Martin Zembaty, and M. Magnor. Towards understanding perceptual differences between genuine and face-swapped videos. *Proceedings of the 2021 CHI Conference on Human Factors in Computing Systems*, 2021. doi: 10.1145/3411764.3445627.
- Yijun Xie. Seeing is no longer believing: a study of deep fake identification ability and its social impact. *Advances in Engineering Innovation*, 2025. doi: 10.54254/2977-3903/2025.28976.
- Chao Xu, Jiangning Zhang, Yue Han, Guanzhong Tian, Xianfang Zeng, Ying Tai, Yabiao Wang, Chengjie Wang, and Yong Liu. Designing one unified framework for high-fidelity face reenactment and swapping. In Shai Avidan, Gabriel J. Brostow, Moustapha Cissé, Giovanni Maria Farinella, and Tal Hassner, editors, *Computer Vision - ECCV 2022 - 17th European Conference, Tel Aviv, Israel, October 23-27, 2022, Proceedings, Part XV*, volume 13675 of *Lecture Notes in Computer Science*, pages 54–71. Springer, 2022a. doi: 10.1007/978-3-031-19784-0_4. URL https://doi.org/10.1007/978-3-031-19784-0_4.
- Ying Xu, Philipp Terhörst, Marius Pedersen, and Kiran B. Raja. Chasing shadows: Solving deepfake detection benchmarks using irrelevant features only. *2025 IEEE 19th International Conference on Automatic Face and Gesture Recognition (FG)*, pages 1–9, 2025. doi: 10.1109/FG61629.2025.11099163.
- Yuting Xu, Jian Liang, Gengyun Jia, Ziming Yang, Yanhao Zhang, and Ran He. Tall: Thumbnail layout for deepfake video detection. In *Proceedings of the IEEE/CVF International Conference on Computer Vision (ICCV)*, pages 22658–22668, 2023.
- Zhiliang Xu, Zhibin Hong, Changxing Ding, Zhen Zhu, Junyu Han, Jingtuo Liu, and Errui Ding. Mobilefaceswap: A lightweight framework for video face swapping. In *Thirty-Sixth AAAI Conference on Artificial Intelligence, AAAI 2022, Thirty-Fourth Conference on Innovative Applications of Artificial Intelligence, IAAI 2022, The Twelveth Symposium on Educational Advances in Artificial Intelligence, EAAI 2022 Virtual Event, February 22 - March 1, 2022*, pages 2973–2981. AAAI Press, 2022b. doi: 10.1609/AAAI.V36I3.20203. URL <https://doi.org/10.1609/aaai.v36i3.20203>.
- Zhiyuan Yan, Yong Zhang, Yanbo Fan, and Baoyuan Wu. Ucf: Uncovering common features for generalizable deepfake detection. In *Proceedings of the IEEE/CVF International Conference on Computer Vision (ICCV)*, pages 22412–22423, 2023a.
- Zhiyuan Yan, Yong Zhang, Xinhang Yuan, Siwei Lyu, and Baoyuan Wu. Deepfakebench: A comprehensive benchmark of deepfake detection. *arXiv preprint arXiv:2307.01426*, 2023b.
- Zhiyuan Yan, Yuhao Luo, Siwei Lyu, Qingshan Liu, and Baoyuan Wu. Transcending forgery specificity with latent space augmentation for generalizable deepfake detection. In *Proceedings of the IEEE/CVF Conference on Computer Vision and Pattern Recognition (CVPR)*, 2024a.

-
- Zhiyuan Yan, Taiping Yao, Shen Chen, Yandan Zhao, Xinghe Fu, Junwei Zhu, Donghao Luo, Chengjie Wang, Shouhong Ding, Yunsheng Wu, and Li Yuan. DF40: toward next-generation deepfake detection. In Amir Globersons, Lester Mackey, Danielle Belgrave, Angela Fan, Ulrich Paquet, Jakub M. Tomczak, and Cheng Zhang, editors, *Advances in Neural Information Processing Systems 38: Annual Conference on Neural Information Processing Systems 2024, NeurIPS 2024, Vancouver, BC, Canada, December 10 - 15, 2024*, 2024b. URL http://papers.nips.cc/paper_files/paper/2024/hash/34239f60eca7ce9bee5280aaf81362d8-Abstract-Datasets_and_Benchmark_s_Track.html.
- Zhiyuan Yan, Jiangming Wang, Peng Jin, Ke-Yue Zhang, Chengchun Liu, Shen Chen, Taiping Yao, Shouhong Ding, Baoyuan Wu, and Li Yuan. Orthogonal subspace decomposition for generalizable ai-generated image detection. In *International Conference on Machine Learning (ICML)*, 2025. Spotlight.
- Shuo Yang, Ping Luo, Chen-Change Loy, and Xiaoou Tang. Wider face: A face detection benchmark. In *Proceedings of the IEEE Conference on Computer Vision and Pattern Recognition*, pages 5525–5533, 2016.
- Wenxuan Zhang, Xiaodong Cun, Xuan Wang, Yong Zhang, Xi Shen, Yu Guo, Ying Shan, and Fei Wang. Sadtalker: Learning realistic 3d motion coefficients for stylized audio-driven single image talking face animation. In *IEEE/CVF Conference on Computer Vision and Pattern Recognition, CVPR 2023, Vancouver, BC, Canada, June 17-24, 2023*, pages 8652–8661. IEEE, 2023. doi: 10.1109/CVPR52729.2023.00836. URL <https://doi.org/10.1109/CVPR52729.2023.00836>.
- Hanqing Zhao, Wenbo Zhou, Dongdong Chen, Tianyi Wei, Weiming Zhang, and Nenghai Yu. Multi-attentional deepfake detection. In *Proceedings of the IEEE/CVF Conference on Computer Vision and Pattern Recognition (CVPR)*, pages 2185–2194, 2021a.
- Tianchen Zhao, Xiang Xu, Mingze Xu, Hui Ding, Yuanjun Xiong, and Wei Xia. Learning self-consistency for deepfake detection. In *Proceedings of the IEEE/CVF International Conference on Computer Vision (ICCV)*, pages 15023–15033, 2021b.
- Wanyi Zhuang, Qi Chu, Zhentao Tan, Qiankun Liu, Haojie Yuan, Changtao Miao, Zixiang Luo, and Nenghai Yu. Uia-vit: Unsupervised inconsistency-aware method based on vision transformer for face forgery detection. In *European Conference on Computer Vision (ECCV)*, pages 391–407. Springer, 2022.

7 ACKNOWLEDGMENTS

N.A.

8 AUTHOR CONTRIBUTIONS

M.P. and V.S.S. conceived and designed the study. M.P. developed the CharadesDF dataset, trained and evaluated all AI detectors, designed and administered the human participant studies, performed all statistical analyses, created all figures and tables, and wrote the manuscript. I.G. generated the deepfake videos for the CharadesDF dataset. V.S.S. supervised the research, secured funding, and provided critical revisions to the manuscript. All authors reviewed and approved the final manuscript.

9 COMPETING INTERESTS

The authors declare no competing interests.

A SUPPLEMENTARY INFORMATION

A.1 RQ1: VIDEO-LEVEL PERFORMANCE

To complement the participant-level analysis, we aggregated predictions at the video level, computing the proportion of correct classifications each video received across all human participants and all AI detectors (Figure 8).

On DF40 (Figure 8A), human accuracy per video ($\mu = 0.742$, $SD = 0.225$) exceeded AI detectors accuracy ($\mu = 0.610$, $SD = 0.141$), paired $t(996) = 17.564$, $p < .001$, $d = 0.556$. The broader distribution of human accuracy ($SD = 0.225$ vs. 0.141 for AI detectors) indicates greater variability in how consistently humans classified individual videos, with some videos achieving near-perfect human consensus while others proved challenging. The gap between humans and AI detectors was more pronounced on CharadesDF (Figure 8B): human accuracy ($\mu = 0.786$, $SD = 0.194$) substantially exceeded AI detectors accuracy ($\mu = 0.537$, $SD = 0.160$), paired $t(778) = 29.432$, $p < .001$, $d = 1.055$.

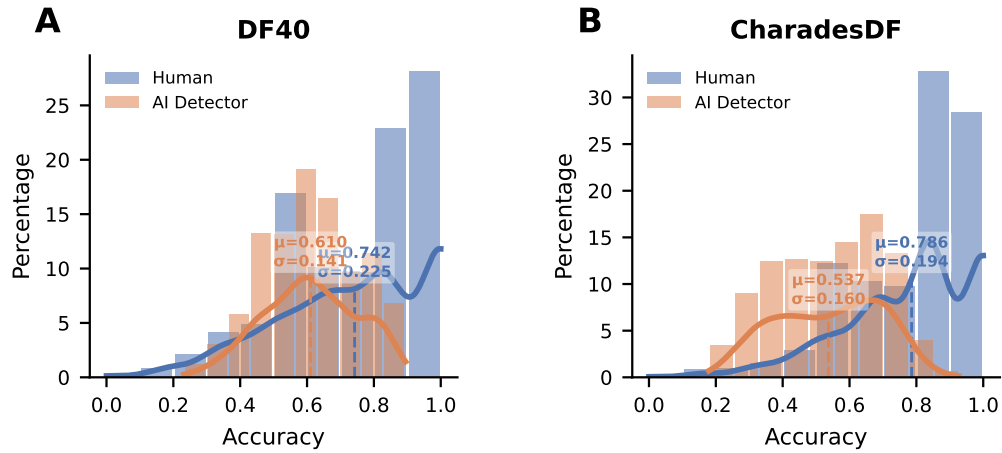


Figure 8: **Distribution of video-level accuracy for human participants and AI detectors.** (A) DF40 dataset. (B) CharadesDF dataset. Each data point represents the proportion of correct classifications for a single video, aggregated across all human participants or AI detectors.

A.2 RQ2: ADDITIONAL ENSEMBLE TECHNIQUES

To assess the robustness of our ensemble findings in RQ2, we evaluated four alternative aggregation strategies beyond the quality-weighted voting presented in Table 1. Soft Mean (Table 11) computes the simple arithmetic average of probability scores across all judges. Soft Median (Table 12) uses the median probability score, which is more robust to outliers. Soft Max (Table 13) takes the maximum probability score across judges, effectively flagging a video as a deepfake if any single judge is highly confident. Hard Ensemble (Table 14) applies majority voting on binarized predictions (threshold = 0.5) rather than aggregating continuous probability scores.

Table 11: **Soft Mean Ensemble.** Values shown as point estimate \pm error. Error represents half-width of 95% bootstrap CI. CFR = Catastrophic Failure Rate. Bold indicates best ensemble performance.

	DF40				CharadesDF			
	Accuracy	F1	AUC	CFR	Accuracy	F1	AUC	CFR
Human (indiv.)	0.743 \pm 0.023	0.759 \pm 0.020	0.823 \pm 0.020	0.190 \pm 0.017	0.784 \pm 0.027	0.783 \pm 0.027	0.846 \pm 0.024	0.171 \pm 0.025
AI detector (indiv.)	0.610 \pm 0.030	0.612 \pm 0.042	0.686 \pm 0.037	0.279 \pm 0.036	0.537 \pm 0.009	0.533 \pm 0.041	0.583 \pm 0.014	0.317 \pm 0.029
Human ensemble	0.881 \pm 0.020	0.881 \pm 0.022	0.948 \pm 0.013	0.020 \pm 0.009	0.928 \pm 0.017	0.926 \pm 0.019	0.975 \pm 0.010	0.012 \pm 0.007
AI ensemble	0.796 \pm 0.025	0.818 \pm 0.025	0.912 \pm 0.017	0.003 \pm 0.004	0.603 \pm 0.034	0.681 \pm 0.034	0.692 \pm 0.034	0.008 \pm 0.006
Hybrid ensemble	0.925 \pm 0.016	0.926 \pm 0.016	0.980 \pm 0.007	0.000 \pm 0.000	0.914 \pm 0.018	0.914 \pm 0.020	0.975 \pm 0.009	0.000 \pm 0.000

Table 12: **Soft Median Ensemble.** Values shown as point estimate \pm error. Error represents half-width of 95% bootstrap CI. CFR = Catastrophic Failure Rate. Bold indicates best ensemble performance.

	DF40				CharadesDF			
	Accuracy	F1	AUC	CFR	Accuracy	F1	AUC	CFR
Human (indiv.)	0.743 \pm 0.023	0.759 \pm 0.020	0.823 \pm 0.020	0.190 \pm 0.017	0.784 \pm 0.027	0.783 \pm 0.027	0.846 \pm 0.024	0.171 \pm 0.025
AI detector (indiv.)	0.610 \pm 0.030	0.612 \pm 0.042	0.686 \pm 0.037	0.279 \pm 0.036	0.537 \pm 0.009	0.533 \pm 0.041	0.583 \pm 0.014	0.317 \pm 0.029
Human ensemble	0.857 \pm 0.022	0.860 \pm 0.023	0.924 \pm 0.016	0.067 \pm 0.015	0.920 \pm 0.018	0.919 \pm 0.020	0.961 \pm 0.013	0.045 \pm 0.014
AI ensemble	0.767 \pm 0.025	0.803 \pm 0.024	0.907 \pm 0.017	0.038 \pm 0.012	0.579 \pm 0.035	0.682 \pm 0.033	0.696 \pm 0.034	0.083 \pm 0.020
Hybrid ensemble	0.903 \pm 0.019	0.906 \pm 0.019	0.974 \pm 0.008	0.006 \pm 0.005	0.910 \pm 0.020	0.910 \pm 0.021	0.966 \pm 0.012	0.001 \pm 0.003

Table 13: **Soft Max Ensemble.** Values shown as point estimate \pm error. Error represents half-width of 95% bootstrap CI. CFR = Catastrophic Failure Rate. Bold indicates best ensemble performance.

	DF40				CharadesDF			
	Accuracy	F1	AUC	CFR	Accuracy	F1	AUC	CFR
Human (indiv.)	0.743 \pm 0.023	0.759 \pm 0.020	0.823 \pm 0.020	0.190 \pm 0.017	0.784 \pm 0.027	0.783 \pm 0.027	0.846 \pm 0.024	0.171 \pm 0.025
AI detector (indiv.)	0.610 \pm 0.030	0.612 \pm 0.042	0.686 \pm 0.037	0.279 \pm 0.036	0.537 \pm 0.009	0.533 \pm 0.041	0.583 \pm 0.014	0.317 \pm 0.029
Human ensemble	0.568 \pm 0.032	0.697 \pm 0.027	0.847 \pm 0.022	0.331 \pm 0.028	0.597 \pm 0.033	0.710 \pm 0.031	0.848 \pm 0.023	0.317 \pm 0.033
AI ensemble	0.499 \pm 0.032	0.666 \pm 0.028	0.812 \pm 0.026	0.501 \pm 0.032	0.496 \pm 0.035	0.663 \pm 0.031	0.675 \pm 0.037	0.504 \pm 0.035
Hybrid ensemble	0.502 \pm 0.032	0.667 \pm 0.028	0.936 \pm 0.014	0.430 \pm 0.032	0.496 \pm 0.035	0.663 \pm 0.031	0.902 \pm 0.022	0.402 \pm 0.033

Table 14: **Hard Ensemble.** Values shown as point estimate \pm error. Error represents half-width of 95% bootstrap CI. CFR = Catastrophic Failure Rate. Bold indicates best ensemble performance.

	DF40				CharadesDF			
	Accuracy	F1	AUC	CFR	Accuracy	F1	AUC	CFR
Human (indiv.)	0.743 \pm 0.023	0.759 \pm 0.020	0.823 \pm 0.020	0.190 \pm 0.017	0.784 \pm 0.027	0.783 \pm 0.027	0.846 \pm 0.024	0.171 \pm 0.025
AI detector (indiv.)	0.610 \pm 0.030	0.612 \pm 0.042	0.686 \pm 0.037	0.279 \pm 0.036	0.537 \pm 0.009	0.533 \pm 0.041	0.583 \pm 0.014	0.317 \pm 0.029
Human ensemble	0.821 \pm 0.026	0.835 \pm 0.025	0.822 \pm 0.025	0.179 \pm 0.026	0.897 \pm 0.021	0.899 \pm 0.022	0.898 \pm 0.021	0.103 \pm 0.021
AI ensemble	0.767 \pm 0.025	0.803 \pm 0.024	0.767 \pm 0.023	0.233 \pm 0.025	0.579 \pm 0.035	0.682 \pm 0.033	0.582 \pm 0.025	0.421 \pm 0.035
Hybrid ensemble	0.719 \pm 0.028	0.780 \pm 0.026	0.900 \pm 0.019	0.059 \pm 0.015	0.597 \pm 0.035	0.709 \pm 0.032	0.890 \pm 0.021	0.050 \pm 0.015

A.3 RQ3: PERFORMANCE CURVES BY QUALITY FEATURE

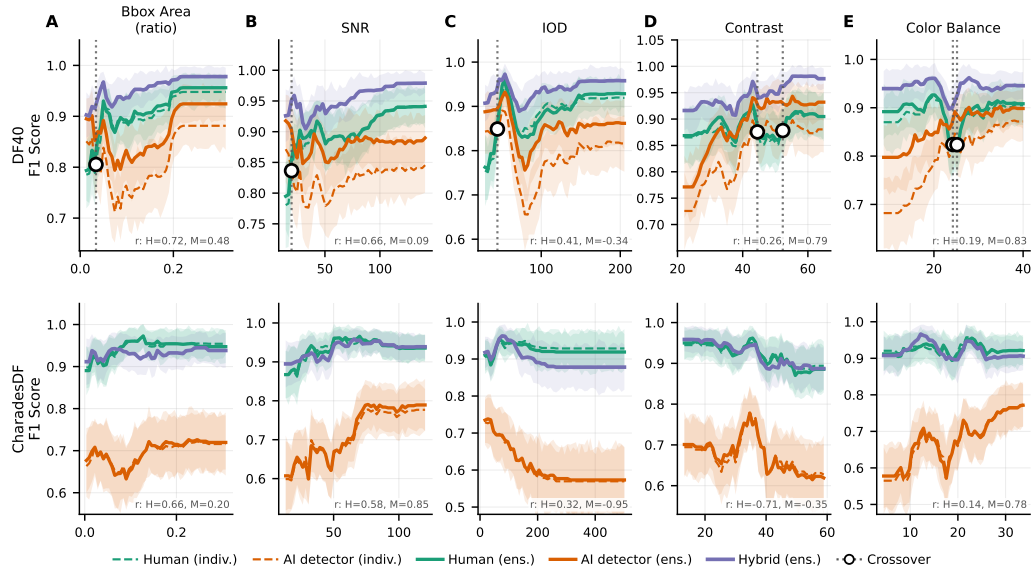


Figure 9: **Detection F1 as a function of quality features.** Smoothed performance curves showing the relationship between quality features and F1 for human individuals (teal, dashed), AI detectors (orange, dashed), human ensembles (teal, solid), AI ensembles (orange, solid), and hybrid ensembles (purple, solid). Shaded regions indicate 95% confidence intervals. We indicate correlations (ρ) in each subplot for both humans (H) and AI detectors (M). Rows correspond to DF40 (top) and CharadesDF (bottom) datasets. Dashed vertical lines indicate human-AI crossovers. **(A)** Bounding box area ratio. **(B)** Signal-to-noise ratio (SNR). **(C)** Inter-ocular distance (IOD). **(D)** Contrast. **(E)** Color balance.

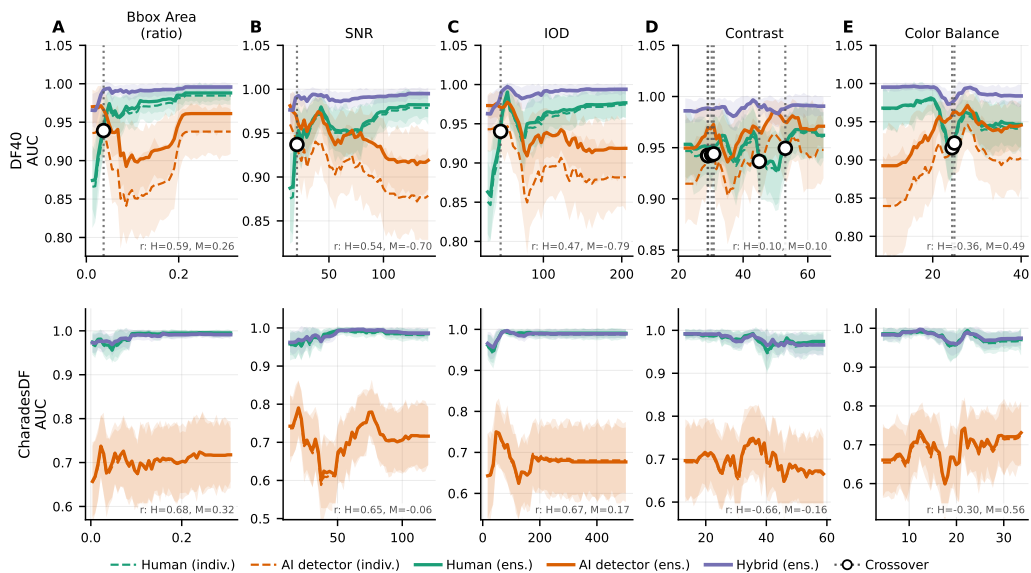


Figure 10: **Detection AUC as a function of quality features.** Smoothed performance curves showing the relationship between quality features and AUC for human individuals (teal, dashed), AI detectors (orange, dashed), human ensembles (teal, solid), AI ensembles (orange, solid), and hybrid ensembles (purple, solid). Shaded regions indicate 95% confidence intervals. We indicate correlations (ρ) in each subplot for both humans (H) and AI detectors (M). Rows correspond to DF40 (top) and CharadesDF (bottom) datasets. Dashed vertical lines indicate human-AI crossovers. (A) Bounding box area ratio. (B) Signal-to-noise ratio (SNR). (C) Inter-ocular distance (IOD). (D) Contrast. (E) Color balance.